ELSEVIER

Deep-Sea Research II 50 (2003) 2971–2996

DEEP-SEA RESEARCH
PART II

www.elsevier.com/locate/dsr2

A nitrate and silicate budget in the equatorial Pacific Ocean: a coupled physical–biological model study

M.-S. Jiang[a,*], F. Chai[a], R.C. Dugdale[b], F.P. Wilkerson[b], T.-H. Peng[c], R.T. Barber[d]

[a] *School of Marine Sciences, 5471 Libby Hall, University of Maine, Orono, ME 04469, USA*
[b] *Romberg Tiburon Center, San Francisco State University, 3152 Paradise Drive, Tiburon, CA 94920, USA*
[c] *NOAA Atlantic Oceanographic and Meteorological Laboratory, Ocean Chemistry Division, 4301 Rickenbacker Causeway, Miami, FL 33149-1026, USA*
[d] *NSOE Marine Laboratory, Duke University, 135 Duke Marine Lab Road, Beaufort, NC 28516, USA*

Received 30 April 2002; received in revised form 15 May 2003; accepted 15 July 2003

Abstract

A coupled physical–biological model was developed to simulate the low-silicate, high-nitrate, and low-chlorophyll (LSHNLC) conditions in the equatorial Pacific Ocean and used to compute a detailed budget in the Wyrtki box (5°N–5°S, 180–90°W) for the major sources and cycling of nitrogen and silicon in the equatorial Pacific. With the incorporation of biogenic silicon dissolution, NH_4 regeneration from organic nitrogen and nitrification of ammonia in the model, we show that silicon recycling in the upper ocean is less efficient than nitrogen. As the major source of nutrients to the equatorial Pacific, the Equatorial Undercurrent provides slightly less $Si(OH)_4$ than NO_3 to the upwelling zone, which is defined as 2.5°N–2.5°S. As a result, the equatorial upwelling supplies less $Si(OH)_4$ than NO_3 into the euphotic zone in the Wyrtki box, having a Si/N supply ratio of about 0.85 (2.5 vs. 2.96 mmol m^{-2} day^{-1}). More $Si(OH)_4$ than NO_3 is taken up with a Si/N ratio of 1.17 (2.72 vs. 2.33 mmol m^{-2} day^{-1}) within the euphotic zone. The difference between upwelling supply and biological uptake is balanced by nutrient regeneration and horizontal advection. Excluding regeneration, the net silicate and nitrate uptakes are nearly equal (1.76 vs. 1.84 mmol m^{-2} day^{-1}). However, biogenic silica export production is slightly higher than organic nitrogen (1.74 vs. 1.59 mmol m^{-2} day^{-1}) following a 1.1 Si/N ratio. In the central equatorial Pacific, low silicate concentrations limit diatom growth; therefore non-diatom new production accounts for most of the new production. Higher silicate supply in the east maintains elevated diatom growth rates and new production associated with diatoms dominate upwelling zone. In contrast, the new production associated with small phytoplankton is nearly constant or decreases eastward along the equator. The total new production has a higher rate in the east than in the west, following the pattern of surface silicate. This suggests that silicate regulates the diatom production, total new production, and thereby carbon cycle in this area. The modeled mean primary production is 48.4 mmol C m^{-2} day^{-1}, representing the lower end of direct field measurements, while new production is 15.0 mmol C m^{-2} day^{-1}, which compares well with previous estimates.

*Corresponding author. Current address: ECOS department, University of Massachusetts Boston, 100 Morrissey Blvd., Boston MA 02125, USA. Tel.: +1-617-287-7416; fax: +1-617-287-7474.

E-mail addresses: mingshun.jiang@umb.edu (M.-S. Jiang), fchai@maine.edu (F. Chai), rdugdale@sfsu.edu (R.C. Dugdale), fwilkers@sfsu.edu (F.P. Wilkerson), tsung-hung.peng@aoml.noaa.gov (T.-H. Peng), rbarber@duke.edu (R.T. Barber).

0967-0645/$ - see front matter
doi:10.1016/j.dsr2.2003.07.006

1. Introduction

The equatorial Pacific is one of the high-nutrient low-chlorophyll (HNLC) areas in the world ocean. The high nutrient often refers to the high concentrations of nitrate and phosphate, yet observed phytoplankton biomass is at a relatively lower level than expected given the optimal light conditions. It has been hypothesized that iron limitation is responsible for this low-chlorophyll biomass (Martin, 1990), in addition to the grazing control by zooplankton (e.g., Cullen et al., 1992; Frost and Frenzen, 1992). The IronEx II experiment clearly demonstrated that iron limits phytoplankton growth in the eastern equatorial Pacific (EEP) (Coale et al., 1996). It has been proposed that the low $Si(OH)_4$ concentration may limit diatom growth as well (Dugdale et al., 1995; Dugdale and Wilkerson, 1998) due to low silicate supply (Ku et al., 1995). The $Si(OH)_4$ concentration within the euphotic zone is relatively low and shows little variability as compared to NO_3, especially in the central equatorial Pacific (CEP). This would establish a possible chemostat-like condition (Dugdale and Wilkerson, 1998) whereby $Si(OH)_4$ regulates diatom growth. Recent field enrichment experiments conducted at 180°W using ^{32}Si as a tracer provided the first ever evidence that $Si(OH)_4$ uptake by diatoms in the equatorial Pacific was severely limited by the availability of silicate (Leynaert et al., 2001), which implies the possible limitation of diatom growth by $Si(OH)_4$.

It is important to understand how the system maintains this low $Si(OH)_4$ condition and its impacts on the new production and carbon cycle, because the equatorial Pacific represents the largest oceanic source of CO_2 to the atmosphere (Takahashi et al., 2002) with new production estimated to account for 18% of the global new production (Chavez and Toggweiler, 1995). The external inputs and the recycling efficiency of nitrogen and silicon in general determine the availability of their dissolved forms. A budget analysis for nitrogen (Toggweiler and Carson, 1995) based on a coupled physical–biological model showed that NO_3 enters the equatorial upwelling system in the far-western Pacific via the Equatorial Undercurrent (EUC). Chai et al. (1996) calculated a NO_3 budget at 140°W on the equator and suggested that about half of the NO_3 supplied by upwelling is carried to the east by the EUC. Consistent with this concept, Dugdale et al. (2002b) provided a budget analysis for the western equatorial Pacific by combining field data and a 3-D physical–biological model (Chai et al., 2003). Their results showed that through western boundary currents, about 70% of the $Si(OH)_4$ flux carried by the EUC comes from the north and the remaining flux from the south, as compared to nearly equal amounts of nitrate supplied from both hemispheres (Dugdale et al., 2002b). It was estimated that the EUC carries a lower $Si(OH)_4$ flux than NO_3 at 160°E, as a result of much lower silicate concentrations in the source water of Southern Ocean origin. This could create the low $Si(OH)_4/NO_3$ ratio (<1) in the CEP and EEP.

The remineralization of organic nitrogen and biogenic silica (BSi) is a critical process for the nutrient recycling efficiency and is not well quantified for the equatorial Pacific. Both the BSi dissolution and nitrogen regeneration depend on a number of factors, including water temperature, nutrient conditions, particle sizes, and zooplankton grazing (Ragueneau et al., 2000; Ward, 2000). The BSi dissolution varies considerably in different areas with the lowest in the Antarctic Ocean and highest in the Sargasso Sea and northwest Africa (Ragueneau et al., 2000). Globally, the export production of BSi at 120 m is estimated to be approximately 50% of the surface production (Tréguer et al., 1998), indicating a moderate efficiency of silicon recycling. Unfortunately, no direct measurement of BSi dissolution in the equatorial Pacific has been made yet. It was estimated that more than 90% of the organic nitrogen was dissolved within the upper 200 m along 150°W (Raimbault et al., 1999), indicating a very efficient nitrogen recycling system. Two other factors may significantly affect the relative efficiency of nitrogen and silicon recycling, which are the Si/N uptake ratio of diatoms and particle sinking velocity. Recent works by Takeda (1998) and Hutchins and Bruland (1998) showed that the diatom uptake Si/N ratio varies from 0.5:1 under Fe-replete conditions to 3:1 under iron-stressed conditions. Values higher than 6:1 were reported

from field enrichment experiments conducted along 170°W in the Antarctic Ocean (Franck et al., 2000). The implication of this is that more silicate than dissolved nitrogen may be taken up by diatoms and exported to deep water in low-iron areas such as the equatorial Pacific. Moreover, the BSi particles could be larger than organic nitrogen due to generally larger sizes of diatoms compared to small phytoplankton and therefore have faster sinking velocities. In brief, the conditions in the equatorial Pacific seem to favor a more efficient recycling of nitrogen than silicon.

In the present study, we use a one-dimensional (1-D) model (CoSINE, Carbon, $Si(OH)_4$, Nitrogen Ecosystem) (Chai et al., 2002; Dugdale et al., 2002a) coupled with a three-dimensional (3-D) ocean circulation model (Li et al., 2001) to study the NO_3 and $Si(OH)_4$ budgets in the equatorial Pacific. This work is a 3-D extension of the 1-D model and provides spatial variability of the ecosystem in the equatorial Pacific. While the concepts in the 1-D models are still adequate in most areas, some of them need to be revised for the far eastern equator or Peru coastal area, where conditions of elevated silicate concentrations seem to deviate from the original 1-D assumptions. In the following paper, brief descriptions of the physical and biological portions of the model are provided. A BSi dissolution model and a Martin function of nitrogen regeneration from organic matter (Martin et al., 1987) have been added to improve the simulation of different nutrient cycling processes. We have calculated a detailed NO_3 and $Si(OH)_4$ budget focusing on the CEP and EEP which can be compared with a NO_3 budget in similar areas computed by Toggweiler and Carson (1995) and a similar budget analysis for the western equatorial Pacific by Dugdale et al. (2002b). The latter suggested that a higher NO_3 flux than $Si(OH)_4$ to the EUC originated the condition of higher NO_3 than $Si(OH)_4$ in the equatorial upwelling zone (EUZ). A detailed discussion about the sources of nutrients and the role of silicon in regulating the new production indicates that nitrogen recycling under current model setting is more efficient than silicon and that this also contributes to the relatively lower $Si(OH)_4$ than NO_3 condition. The results further suggest that silicate availability may regulate the diatom production and hence the total new production in the equatorial Pacific.

2. Model description

2.1. Physical model

The physical model used is the NCAR climate ocean model (NCOM) (Gent et al., 1998), which is a modified version of GFDL Modular Ocean Model (MOM) 1.0 (Pacanowski et al., 1991). We use the version of NCOM configured for the Pacific Ocean by Li et al. (2001). The non-local KPP mixing scheme developed by Large et al. (1994) is adapted to better capture the small-scale physical processes within the upper mixed layer, interior internal waves, and double diffusion activities. Horizontally, the Gent and McWilliam (1990) skew-flux parameterization scheme is used to create the realistic isopycnal mixing. A third-order upwind differencing scheme (Holland et al., 1998) is used to compute all tracers including temperature, salinity and biochemical components. The horizontal and vertical background mixing coefficients are chosen to be 2×10^6 and 0.1 $cm^2\ s^{-1}$, respectively. The low value of the vertical background mixing coefficient is important to maintain a realistic vertical structure of tracers in the thermocline. The vertical viscosity is chosen to be 1 $cm^2\ s^{-1}$, an order of magnitude larger than the background mixing, while the horizontal viscosity is 5×10^6 $cm^2\ s^{-1}$.

The full model domain is between 45°S and 65°N, 100°E and 70°W, with realistic coastal geometry and bottom topography. The southern boundary is closed with a solid wall at 45°S. The longitudinal resolution is 2° everywhere, while the latitudinal resolution is 0.5° within 10°S and 10°N, tapering off to 2° at both the north and south boundaries. There are 40 vertical layers, with 23 levels located in the upper 400 m. With relatively high resolution in both the horizontal and vertical coordinates, the model reproduces the equatorial current system reasonably well, including the North Equatorial Countercurrent (NECC), South Equatorial Current (SEC) and the EUC.

The current system, to a large extent, governs the structure and transport of passive tracers in the upper layer of the equatorial Pacific. More importantly, high vertical resolution enables us to describe accurately biogeochemical processes, which mainly occur in the upper ocean.

The model is forced with the monthly Comprehensive Ocean Atmosphere Data Set (COADS). The heat flux is based on the bulk formulation that consists of incoming short-wave radiation, outgoing long-wave radiation, sensible and latent heat fluxes. The detailed calculations of these fluxes can be found in Li et al. (2001). The sea-surface salinity is restored to the monthly Levitus climatology (Levitus et al., 1994) with a restoring time scale of 30 days.

2.2. Biological model

The biological model is based on the 1-D model developed by Chai et al. (2002) and Dugdale et al. (2002a). The model has ten components representing two sizes of phytoplankton, small phytoplankton cells (S_1) (less than 5 μm in diameter) and diatoms (S_2), micro- and meso-zooplankton (Z_1 and Z_2), nonliving detrital nitrogen and silica (DN and DS_i), dissolved silicic acid (silicate; $Si(OH)_4$), two forms of dissolved inorganic nitrogen: nitrate (NO_3) and ammonium (NH_4), and total CO_2 (TCO_2). The photosynthetically available radiation (PAR) uses 50% short-wave radiation from COADS to account for the 400–700 nm visible light range. Different from the 1-D model (Chai et al., 2002), no diel cycle of solar radiation is simulated and the PAR is applied uniformly to the ocean 24 h a day, which attenuates with depth due to water absorption and scattering. The model has a fixed euphotic depth of 112 m, below which it is assumed that no photosynthetic activity takes place. Some modifications are made for the biological parameters (Table 1) in the current simulation. The formulations used for the biological processes are exactly the same as in Chai et al. (2002), except for nitrogen remineralization and BSi dissolution (see below). Based upon a similar 3-D physical–biological model configuration to this paper, Chai et al. (2003) simulated ecosystem response to the decadal variation in the Pacific Ocean. More detailed descriptions of the biological model can be found in the 1-D paper by Chai et al. (2002).

2.2.1. The remineralization of organic nitrogen and nitrification

The remineralization of organic nitrogen is primarily biological with a rapid production of NH_4 and urea through zooplankton grazing in the euphotic zone and bacterial decomposition of organic matter down below. The nitrification through the bacterial oxidation of NH_4, which mainly occurs below the euphotic zone, further transforms the NH_4 to NO_3. Within the euphotic zone, zooplankton excretion is represented as constant fractions (reg1 and reg2, see Table 1) of zooplankton biomass. In addition, a low ammonia regeneration (0.025 day^{-1}) of organic matter is used. Both processes are subject to temperature (Q10) effect (Eppley, 1972). Below the euphotic zone, we used an empirical power law suggested by Martin et al. (1987), which has been widely used in biogeochemical models (e.g., Sarmiento et al., 1993; Chai et al., 1996; Christian et al., 2001). Specifically, assuming that the export flux of organic nitrogen at 112 m is f_{112}, then the specific regeneration rate of NH_4 at depth z is,

$$\mathrm{NH_4\ Regeneration} = \begin{cases} 0.025\exp(0.069(T-25))\mathrm{DN} & z<112\ \mathrm{m}, \\ f_{112}\left(\dfrac{z_2}{112}\right)^{-b} - f_{112}\left(\dfrac{z_1}{112}\right)^{-b} & z>112\ \mathrm{m}, \end{cases} \quad (1)$$

where T is water temperature and b is the index of power law, DN is the concentration of detritus, and Z_1 and Z_2 are the top and bottom of model layer, respectively. Results from US JGOFS surveys in the equatorial Pacific showed that b varies from 0.60 to 0.81 between 5°N and 5°S (Berelson, 2001), and is less than the original value of 0.858 suggested by Martin et al. (1987) in the northeast Pacific. A median value of 0.72 is used in the current model.

The ammonium oxidation to NO_3 involves two steps: ammonium oxidation to nitrite (NO_2), and nitrite oxidation to nitrate (NO_3). Within the

Table 1
Parameters of the biological model

Parameters	Symbol	1-D[a]	This study	Unit
Averaged surface noontime irradiance	I_o^{Noon}	410	Obs.	W m^{-2}
Light attenuation due to water	k_1	0.046	0.033	m^{-1}
Light attenuation by phytoplankton	k_2	0.03	0.03	m^{-1} (mmol m^{-3})$^{-1}$
Initial slope of the P–I curve	α	0.025	0.025	day^{-1} (W m^{-2})$^{-1}$
Maximum specific growth rate of small phytoplankton	$\mu 1_{\max}$	2.0	1.8	day^{-1}
Ammonium inhibition parameter	ψ	5.59	8.0	(mmol m^{-3})$^{-1}$
Half-saturation for nitrate uptake	K_{NO_3}	0.5	1.0	mmol m^{-3}
Half-saturation for ammonium uptake by small phytoplankton	K_{NH_4}	0.05	0.05	mmol m^{-3}
Maximum specific growth rate of diatoms	$\mu 2_{\max}$	3.0	2.0	day^{-1}
Half-saturation for silicate uptake	$K_{Si(OH)_4}$	3.0	3.5	mmol m^{-3}
Half-saturation for ammonium uptake by diatoms	$K_{S_2\text{-}NH_4}$	1.0	0.35	mmol m^{-3}
Diatoms sinking speed	W_1	1.0	1.0	m day^{-1}
Microzooplankton maximum grazing rate	$G1_{\max}$	1.35	1.8	day^{-1}
Half-saturation for microzooplankton ingestion	$K1_{gr}$	0.5	0.5	mmol m^{-3}
Microzooplankton excretion rate to ammonium	reg_1	0.2	0.2	day^{-1}
Mesozooplankton maximum grazing rate	$G2_{\max}$	0.53	0.53	day^{-1}
Mesozooplankton assimilation efficiency	γ_1	0.75	0.835	
Half-saturation for mesozooplankton ingestion	$K2_{gr}$	0.25	0.20	mmol m^{-3}
Diatom specific mortality rate	γ_4	0.05	0.1	day^{-1}
Small phytoplankton specific mortality rate	γ_3	NA	0.1	day^{-1}
Mesozooplankton specific mortality rate	γ_2	0.05	0.005[b]	day^{-1}
Mesozooplankton excretion rate to ammonium	reg_2	0.1	0.17	day^{-1}
Grazing preference for diatoms	ρ_1	0.7	0.7	
Grazing preference for microzooplankton	ρ_2	0.2	0.15	
Grazing preference for detritus	ρ_3	0.1	0.15	
Detritus sinking speed	W_2	10.0	10.0	m day^{-1}
Diatom Si/N uptake ratio	Si_2N	1.0	1.5	
Nitrification rate within euphotic zone	γ_5	NA	0.025	day^{-1}
Index of Martin function	b	NA	0.75	

[a] CoSINE model (Chai et al., 2002).
[b] A linear dependence of zooplankton mortality on the zooplankton biomass was used: $\gamma_0 = \gamma_2^* Z_2$.

euphotic zone, very low nitrification rates occur (Dore and Karl, 1996; Ward, 2000). Therefore, we model the combined effect of these two steps with a specific oxidation rate (0.025 day^{-1}) within the euphotic zone and a higher rate below the euphotic zone (0.1 day^{-1}).

2.2.2. Dissolution of BSi

The BSi dissolution rate varies significantly with area and depth and depends strongly on the water temperature, among other factors (Ragueneau et al., 2000). For simplicity, we only considered temperature effects and chose the following formulation:

$$\text{Dissolution} = (0.19T/25 + 0.01) \times \exp(0.069(T - 25)). \quad (2)$$

This formulation has a similar shape to the Arrhenius function used by Gnanadesikan (1999). This dissolution scheme has a rate of 0.2 day^{-1} at temperature of 25°C, which is on the higher end of the observed 0.01–0.2 day^{-1} in the Sargasso Sea (Brzezinski and Nelson, 1995) and 0.1 day^{-1} reported in the neighboring Peruvian coast (Nelson et al., 1981). The dissolution rate decreases to 0.05 day^{-1} at 200 m where the annual

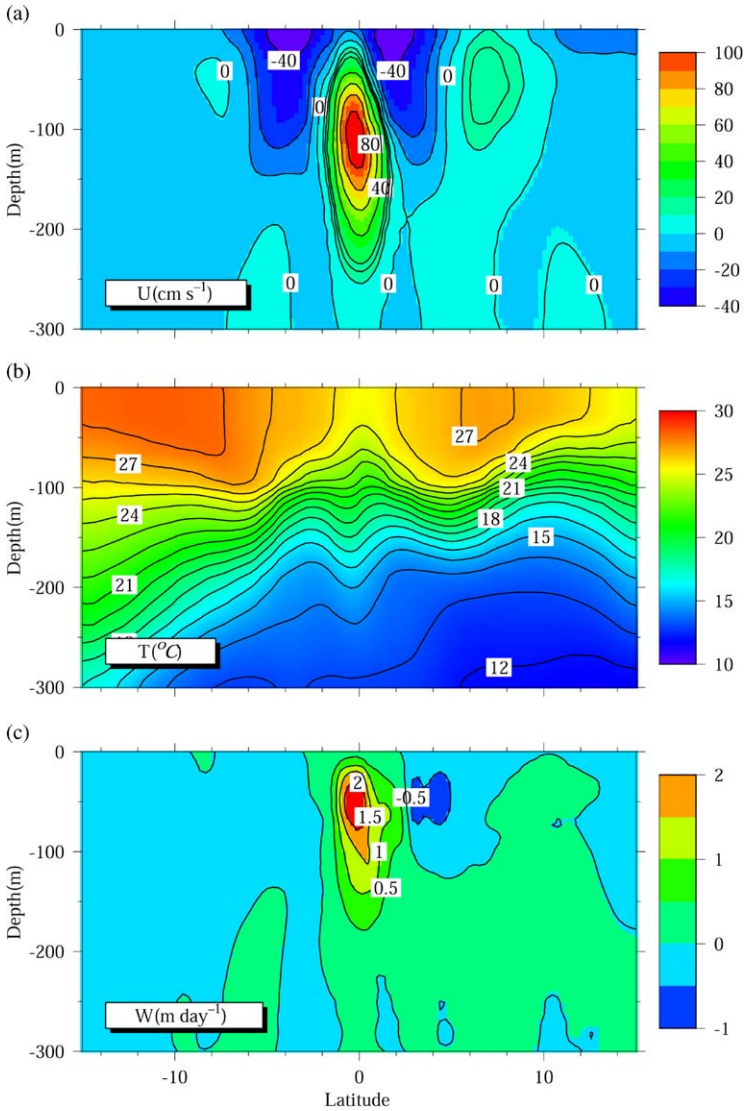

Fig. 1. Annual mean of physical conditions along 140°W: (a) zonal velocity; (b) temperature; and (c) vertical velocity.

mean temperature ranges from 14°C to 16°C within equatorial band (Fig. 1) and the background rate of 0.01 day^{-1} at depth. Therefore, the dissolution rate at 200 m is about one-fourth of the surface value with a time scale of 20 days. With a particle sinking velocity of 20 m day^{-1}, these imply a roughly 100 m length scale at the surface and about 400 m within the thermocline.

In effect, we can expect that the majority of BSi dissolution in our model occurs within the euphotic zone and decreases rapidly with depth, consistent with measured high dissolution within the upper 50–100 m and very low values below (e.g., Nelson and Goering, 1977), though the near-surface profile here may not be realistic due to a strict temperature dependence (see discussion in Section 4.1). In comparison, nitrification will have a maximum near the bottom of the euphotic zone, while nitrogen regeneration to NH_4 mainly occurs within the euphotic zone. In the ocean, the

$Si(OH)_4$ and NO_3 profiles reflect these differences in remineralization processes. The $Si(OH)_4$ concentration increases steadily with depth to very high values, while NO_3 increases to maximum values at fairly shallow depths (about 500 m) and fails to increase with increased depth.

2.2.3. Iron limitation and Si/N uptake ratio by diatoms

The iron limitation is represented in the model as a constant low initial slope (α_{max}) of the P vs. I curve for photosynthesis (Chai et al., 2002), which is based on measurements made during EqPac Survey II (Lindley et al., 1995). No direct linkage has been made between changes in iron supplies due to upwelling or aeolian dust and changes of phytoplankton growth. Another possible effect of iron limitation is the influence of low iron conditions on the diatom uptake ratio of silica and nitrogen. We used a fixed median value of $Si/N = 1.5:1$ in the current model, which is higher than the global consensus 1:1 (Brzezinski, 1985) but lower than 2:1 reported by Takeda (1998) in the Southern Ocean. This is a lower limit of reported Si/N values under iron deplete conditions (Takeda, 1998; Hutchins and Bruland, 1998). Therefore, the Si uptake in the current simulation may be under-estimated. Again, there is no direct linkage in the model between possible iron supplies with changes of Si/N uptake ratio by diatoms. Therefore, the current implementation should be viewed as a mean realization of iron limitation, which is consistent with the concept of climatological modeling. The responses of the system with iron addition can be found in the 1-D paper (Chai et al., 2002), as well as in the previous similar 3-D ecosystem modeling study (Chai et al., 1996, 1999). More discussion is in Section 4.3.

2.3. Initialization and boundary treatments

The model was initialized with the climatological temperature and salinity (Levitus et al., 1994) and nutrients (NO_3 and $Si(OH)_4$) (Conkright et al., 1994). North of the equator, the $Si(OH)_4$ concentrations in the data set are overall higher than the direct field measurements without any interpolation (e.g., Carr et al., 1992; Murray et al., 1995). Therefore, a 20% reduction was made between 10°N and 20°N, while the rest of the domain was kept unchanged. There is no material flux on the boundaries, since the model domain is closed with solid boundaries. To best represent sources of nutrients from sub-polar areas, two sponge layers covering 10° each were implemented at both the north and south boundaries. The physical model was spun up for 15 years to reach a quasi-steady state in the upper ocean. From that point on, the coupled model was integrated for 20 years to reach a quasi-steady state for the upper layer. Although the deep ocean was still adjusting, we believed that it does not affect the upper layer significantly. The results from the final year integration are used in the present analysis.

3. Results

3.1. Hydrological conditions and circulation

The equatorial Pacific current system consists of four major currents, the SEC, the North Equatorial Current (NEC), the NECC, and the EUC (Wyrtki and Kilonsky, 1984; Murray et al., 1995). As driven by the trade winds, the SEC straddles the equator with two main axes, the northern one centered at 2–3°N and restricted to 4°N by the NECC. The southern branch of the SEC is slightly weaker and broader. The meeting place of the NECC and SEC, around 4–6°N, usually exhibits strong tropical instability waves (TIWs), which have significant implications for biogeochemical processes (Archer et al., 1997). At 140°W, the EUC has its core at a depth of around 120 m with a maximum velocity of about 100 cm s^{-1}. Its main axis is displaced slightly south of the equator. Associated with the equatorial divergence, two meridional circulation cells are persistent on both sides of the equator, both having poleward flow near the surface and equatorward flow below the mixed layer. Below the SEC, two branches of the subsurface countercurrent also are clearly seen between 4–8°S and 3–7°N, respectively. The northern branch is connected with both the EUC and NECC as reported by Wyrtki and Kilonsky (1984) and more intense than the southern branch.

Overall, the model reproduces all of these annual mean circulation and hydrological conditions as shown in Fig. 1. There are small differences in the magnitudes and locations of currents, however. For example, the modeled NECC is weaker than the observed, with a maximum of about 15 cm s^{-1} as compared to the measured 40 cm s^{-1} during the Hawaii-Tahiti Shuttle experiment (Wyrtki and Kilonsky, 1984), which was calculated from CTD data covering approximately 1 year period 1979–1980 and therefore may not represent climatological conditions. The modeled NEC is weaker than the observed as well, and more confined to the surface. The model also simulated the transport of all major currents reasonably well. The EUC annual mean flux is roughly 31 Sv at 180°W, which compares well with previous modeled results (approximately 30 Sv) at this longitude (e.g., Lu et al., 1998) and is consistent with the measured 25 Sv at 155°E (Butt and Lindstrom, 1994). At 10°N the southward interior transport from the subtropical north Pacific is located mainly below the mixed layer and above the 25.9 isopycnal (roughly 200 m), with a flux of about 4.6 Sv. The northward flux from the Southern Ocean at 10°S is deeper between the base of the mixed layer and the 26.1 isopycnal with a larger flux (13.8 Sv). These meridional fluxes compare well with geostrophic estimates by Johnson and McPhaden (1999) of 5.5 Sv at 8°N and 14 Sv at 8°S.

The equatorial Pacific has strong upwelling near the equator in the upper 250 m and downwelling off the equator (Philander, 1990). As shown in Fig. 1c, the upwelling is in general confined to a 2.5°N–2.5°S latitudinal band (so-called equatorial upwelling zone, EUZ). The downwelling centered at 4°N has a subsurface maximum of more than 1 m day^{-1}, obviously stronger than its southern counterpart, which is centered at 5°S and less than 0.5 m day^{-1}. Weak Ekman pumping associated with the divergence of the NECC and NEC occurs throughout the upper 300 m. The upwelling at 50 m in the area of 3.6°S–5.2°N, 170–95°W is estimated as 62 ± 16 Sv based on hydrological data in 1991–1999 (Johnson et al., 2001). Our modeled estimate in the same area is 40 Sv, which is on the lower end of the observation. Below the EUC core, the model shows weak upwelling confined to a narrow band of 1°N–1°S. Several references based on different measurements made at different times gave contradicting estimates at this depth (e.g., Bryden and Brady, 1985; Weisberg and Qiao, 2000).

3.2. Nutrient conditions

The annual mean nutrient (NO_3, $Si(OH)_4$ and NH_4) concentrations along 140°W are shown in Fig. 2. Consistent with stronger Ekman pumping on the north below the NEC (Fig. 1b), NO_3 and $Si(OH)_4$ have a higher ridge at about 80 m at 10°N compared to 120 m at 3°S. As a result, the nutrient fields below the euphotic layer showed strong

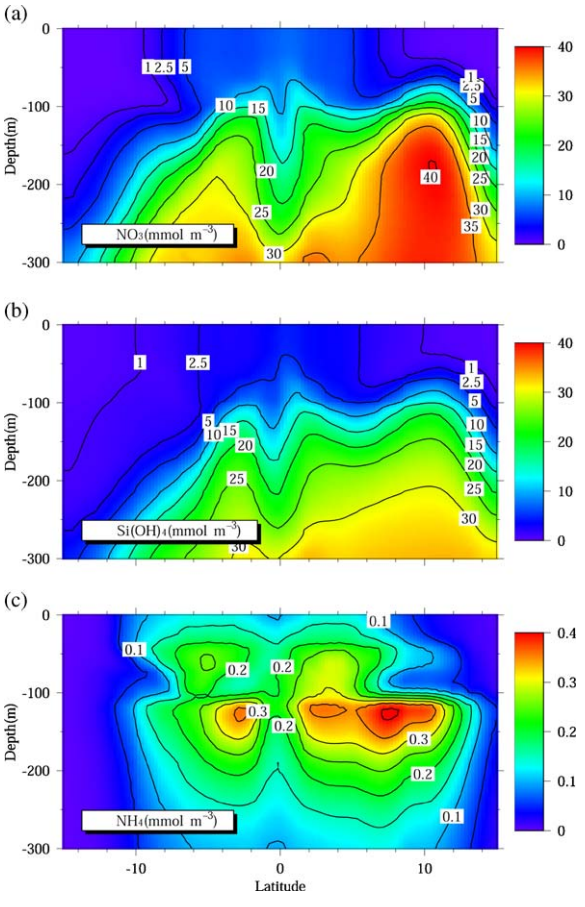

Fig. 2. Annual mean of nutrients at 140°W: (a) nitrate; (b) silicate; and (c) ammonium.

asymmetry over the equator. This feature was also seen in the western equatorial Pacific during the WEPOCS III cruise (Dugdale et al., 2002b). Within the euphotic layer, the $Si(OH)_4$ distribution is generally symmetrical about the equator, while NO_3 has higher concentrations to the south than north. The observations of the Hawaii-Tahiti Shuttle experiment (Wyrtki and Kilonsky, 1984) also showed much higher NO_3 to the south and the 2.5 mmol m^{-3} isopleth outcrops nearly at the equator from the north. However, Carr et al. (1992) observed an almost symmetrical NO_3 distribution during WEC88. Both observations showed a symmetrical distribution of $Si(OH)_4$ about the equator. The modeled ammonium field shows a clear subsurface maximum centered at 5°S and 3°N, respectively. Both maxima were also observed off the equator during WEC88 (Wilkerson and Dugdale, 1992), EqPac Survey I and II (Murray et al., 1995) and OLIPAC (Raimbault et al., 1999), though the locations of the maxima varied considerably. The maxima from the observations were deeper (around 80–120 m) and concentrations were higher than the model results (Fig. 2), up to 1.0 mmol m^{-3} and reaching as far as 10°S. The observed NH_4 concentrations in the north were comparable with modeled results. Near the base of the euphotic layer, the modeled NH_4 to the south appears to be lower than the observed, which may be due to inadequate parameterization of metabolic processes. However, this will not have much impact on the primary production and phytoplankton biomass within the equatorial band since the production occurs within the euphotic layer and NH_4 concentration is much higher than the half-saturation concentration (0.05 mmol m^{-3}) for the small phytoplankton growth.

These physical and nutrient features are typical in the equatorial Pacific, with weaker currents and higher nutrients further east in general. Along with the shoaling of the thermocline to the east, the EUC also lifts upward with its core located at about 70 m near the Peruvian coast compared to 200 m west of 165°E. East of 120°W, the south recirculation becomes stronger than the north recirculation cell. In association with the shallower

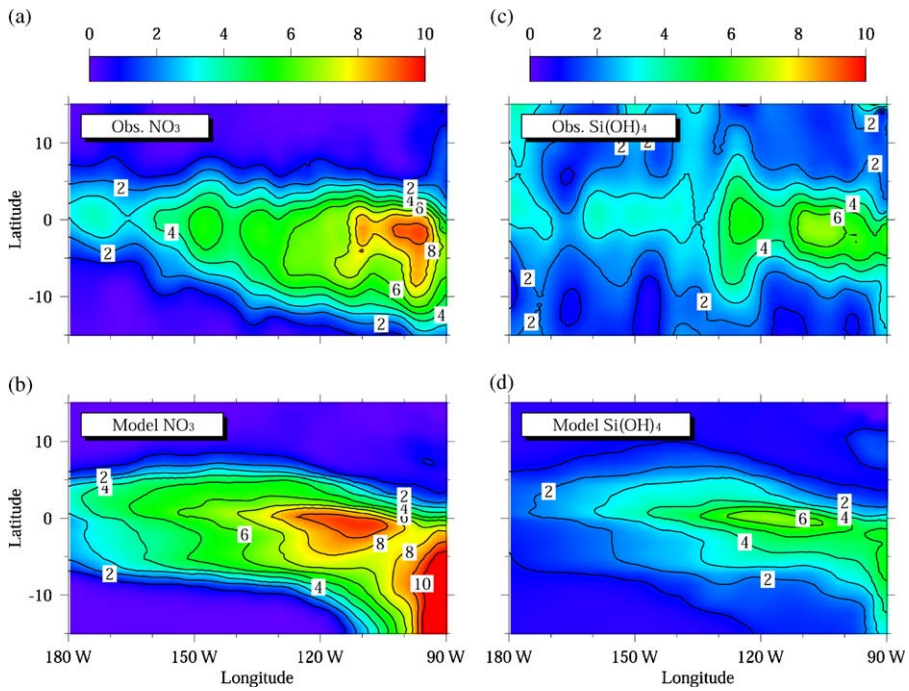

Fig. 3. Comparisons of modeled annual mean of surface nutrients (mmol m^{-3}) in eastern Equatorial area and climatological data from WOA98: (a) observed NO_3; (b) modeled NO_3; (c) observed $Si(OH)_4$; and (d) modeled $Si(OH)_4$.

EUC, the high-nitrate band becomes much broader and more heavily placed in the south (Figs. 3a and c) where the SEC carries Peru upwelling water to the west. Silicate concentration increases eastward as well, but the high silicate band is still limited to the 5°N–5°S band (Figs. 3b and d).

In general, the surface NO_3 concentration in the eastern part of the high-nutrient tongue is about 2 mmol m^{-3} higher than Si(OH), as evident in the modeled results and World Ocean Atlas (Conkright et al., 1998, WOA98 hereafter) (Fig. 3). The pattern of modeled surface nutrients is in good agreement with the data except for the southeast corner where the modeled NO_3 concentration is much higher than the observed. The low light acclimation assumption consistent with general Fe-limitation conditions may impose too strong a constraint in this area because persistent upwelling may provide more iron for phytoplankton growth. In the CEP, the westward decrease of $Si(OH)_4$ is faster than the observed (Fig. 9a). By performing data quality control based on regression of nutrients to temperature, Louanchi and Najjar (2000) recompiled WOA98 and showed broader high-nutrient tongue but lower-nutrient level than both our modeled results and WOA98. Averaging over the Wyrtki box (5°N–5°S, 180–90°W), the modeled profile of $Si(OH)_4$ agrees very well with WOA98 within the upper 200 m (Table 3). To understand the upwelling ratio of nitrate and silicate, we performed regressions for averaged nutrients in the EUZ. Between 100 and 300 m, a depth range in which the nutrient gradient is critical to the upwelling supply, the regression slope of $Si(OH)_4$ against NO_3 is 0.93 in the model, comparing well with 0.92 from WOA98. A Si/N ratio < 1 is indicative of more nitrate supply to the euphotic zone.

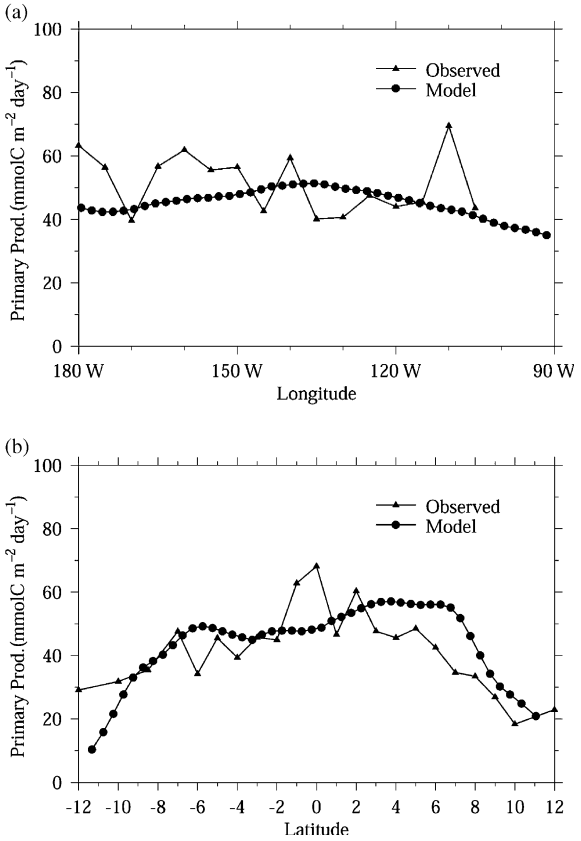

Fig. 4. Comparisons of depth integrated primary production with observations. The observed data were collected by Duke University, including primary productivity data sampled during 40 cruises in the equatorial Pacific between 1983 and 1996. (a) Depth-integrated primary production over 5°N–5°S from the model and observations. The modeled production were averaged over 5°N–5°S, whereas the observations were derived by binning production observed between 5°N and 5°S into 5° longitudinal intervals. (b) Integrated primary production along 140°W from model and observation. The modeled production were along 140°W, while the observed data were derived by binning observations made between 150–130°W into 1° latitudinal intervals, but excluding the measurements made near Marquesas Islands.

3.3. New and primary production

To validate the model results further, the integrated primary production within the euphotic zone is presented in Fig. 4, in which a constant carbon to nitrogen ratio (6.625:1) has been used to convert the production from nitrogen units into carbon units. This conversion applies throughout the remaining discussion. Overall, the modeled mean primary production within 5°N–5°S (Fig. 4a) is consistent with, but often somewhat lower than, the observed data. The modeled primary production along 140°W when compared with the zonal mean from historical observations made between 150°W and 130°W (Fig. 4b) agrees with the observations very well at most stations.

Table 2
Comparisons of modeled production with observations and other modeled results (mmol C m^{-2} day^{-1})

References		New production	Primary production	Measurement area and period
Observations	Chavez et al. (1996)		75	Wyrtki box (EqPac I & II)
	Barber et al. (1996)		91	5°N–5°S, 140°W (EqPac II)
	Pena et al. (1990)		56.7	7°N–6°S, 135°W (April 1988)
	Dugdale et al. (1992)	5	35.7	6°N–8°S, 150°W (Feb.–Mar. 1988)
	MCarthy et al. (1996)	13		5°N–7°S, 140°W (EqPac II)
	Raimbault et al. (1999)	10–12.9	50.8–90.8	1°N–5.5°S, 150°W (OLIPAC)
Models	Chai et al. (1996)	16.4	50	Wyrtki box (3-D model)
	Toggweiler and Carson (1995)	22	99	Wyrtki box (3-D model)
	Leonard et al. (1999)	56	117–137	0°, 140°W (Fall, 1992) (1-D model)
	Christian et al. (2001)		181	(1°N–1°S, 140°W) (3-D model)
	Chai et al. (2002)	13	64	Wyrtki box (1-D CoSINE model)
	This study	15.0	48.4	Wyrtki box (3-D model)

The modeled production, however, is significantly lower than the observed south of 9°S.

Table 2 shows comparisons between the modeled production in the Wyrtki box and the observational and other modeling estimates. Our primary production of 48.4 mmol C m^{-2} day^{-1} is in the range of single cross-section measurements made along 140°W during EqPac Survey II (Barber et al., 1996) and 150°W during WEC88 (Dugdale et al., 1992; Peña et al., 1990), respectively, but lower than EqPac survey estimates over the Wyrtki box (Chavez et al., 1996). Integrated over the box, the model gives a total primary production of 2.2 Gt C yr^{-1}, which is on the higher end of estimates (0.80–1.9 Gt C yr^{-1}) made by Chavez and Barber (1987) (see their Table 7). The modeled new production is about the same as EqPac Survey II (McCarthy et al., 1996), but higher than the WEC 88 (Dugdale et al., 1992). The integrated new production (0.72 Gt C yr^{-1}) represents lower value compared to previous estimates 0.7–1.0 Gt C yr^{-1} (see Chai et al., 1996). Both new and primary production are consistent with the estimates from the five-component 3-D model (Chai et al., 1996) and the recent 1-D CoSINE model (Chai et al., 2002) but lower than predictions by other models (Toggweiler and Carson, 1995; Leonard et al., 1999; Christian et al., 2001). On average, diatoms contribute 37% of new production and 25% of primary production. Averaged over 2°N–2°S, these percentages increase to 46% and 31%, respectively.

3.4. Nitrate and silicate budget

A detailed NO_3 and $Si(OH)_4$ budget is shown in Fig. 5, which includes major advective fluxes, phytoplankton uptake and nutrient regeneration. Vertical fluxes include the contributions from vertical mixing. The latitudinal range (5°N–5°S) of these boxes shown in Fig. 5 covers the EUC and part of the SEC. Vertically the middle two boxes cover the majority of the EUC path and therefore are roughly referred to as the EUC. For convenience, we refer hereafter to the equatorial areas (180°W, 135°W) and (135°W, 90°W) as CEP and EEP, respectively. In order to clarify the major pathways of nutrient transport within the EUZ (2.5°N–2.5°S), we also computed the nutrient transport for the EUZ as shown in Fig. 6. This figure consists of two upper boxes for the mixed layer (upper 50 m) and two lower boxes bounded by the base of mixed layer and a sloping bottom, representing roughly the bottom of the EUC. Specifically, the bottom box of the CEP (left side) covers more than 90% of the EUC in terms of volume transport, while the bottom box in the EEP (right side) covers nearly the entire EUC consistent with steeper sloping of the EUC. In both Figs. 5 and 6, we did not separate the upper and lower EUC as both Toggweiler and Carson

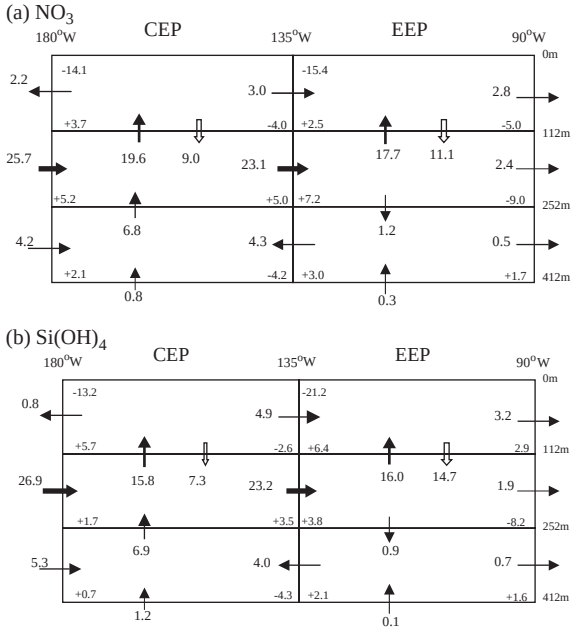

Fig. 5. (a) Nitrate and (b) silicate budgets (10^4 mol s^{-1}). Horizontally, we use the same boxes as Toggweiler and Carson (1995), i.e. we divided the Wyrtki box (5°N–5°S, 180–90°W) into two boxes: the west box (5°N–5°S, 180–135°W) and the east box (5°N–5°S, 135–90°W). Geographically, the west box represents the CEP, while the east box is the EEP. Vertically, we have three boxes bounded at 0, 112, 252 and 412 m, respectively. The top box is consistent with the euphotic layer to highlight the entire biological activities, which includes part of the EUC. The solid arrows represent advection and diffusion fluxes, open arrows represent sinking fluxes of detritus. The net meridional fluxes are displayed on the lower right corner of each box. The biological uptake in the top layer and regeneration in each box are shown on the upper left corner and lower left corner, respectively. Those numbers indicated by open arrows at 112 m are biogenic export production. Note that the export fluxes at 252 and 412 m are not shown.

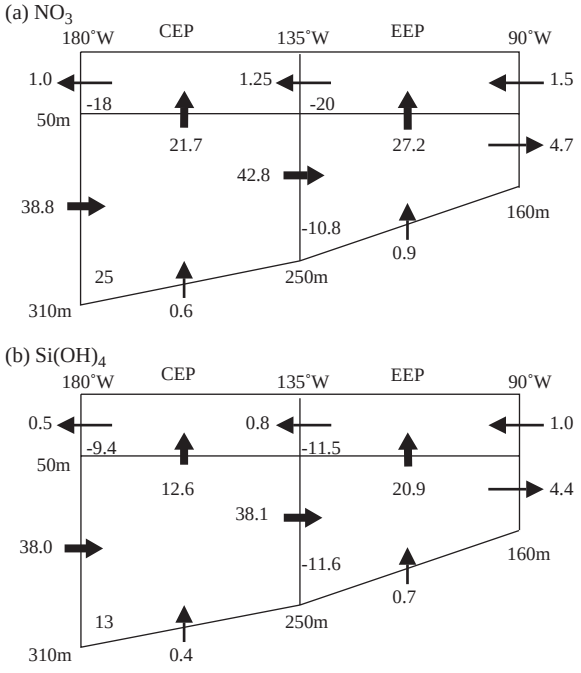

Fig. 6. The NO_3 (a) and $Si(OH)_4$ (b) fluxes in the EUZ(2.5°N–2.5°S) (10^4 mol s^{-1}). The top boxes represent the mixed layer while the bottom boxes show the path of the EUC, which shoals along with the path. The latitudinal band for these boxes is 2.5°N–2.5°S. As in Fig. 5, those numbers with the arrows represent nutrient fluxes, except that the meridional fluxes are marked on the lower left of the boxes now.

(1995) and Dugdale et al. (2002b) did. In this section, we mainly discuss the budget in Fig. 5, but refer to the EUC path in Fig. 6.

3.4.1. Nutrient transports

It is clear that the EUC carries most of the nutrient fluxes, which mostly upwell to the euphotic zone before reaching the eastern boundary (Fig. 5). Below the EUC, nutrients are transported with much smaller fluxes, having an eastward flux at the dateline and nearly equal westward fluxes at 135°W (Fig. 5). Within the euphotic layer, the SEC tends to balance the EUC underneath, leaving a very small net exchange on the dateline and 90°W. At 135°W there are small eastward fluxes (3.0×10^4 mol s^{-1} for NO_3 and 4.9×10^4 mol s^{-1} for $Si(OH)_4$), implying that the CEP actually feeds nutrients to the EEP within the euphotic zone. This result is consistent with previous model results by Chai et al. (1996), but could be sensitive to the depth where the EUC and SEC meet. In our model, this depth is about 20 m, which is on the lower end of a sharp change from 10 m at about 1°S to 75 m at the equator, observed by the Hawaii-Tahiti Shuttle experiment (Wyrtki and Kilonsky, 1984), but shallower than the 70 m seen during EqPac Survey II (Murray et al., 1995). The direction of the net fluxes is also dependent on the vertical gradient of nutrients, which is a combined result of upwelling gradient, biological uptake and regeneration. At the

dateline, slightly more $Si(OH)_4$ (1.1×10^4 mol s^{-1}) than NO_3 is carried eastward below the euphotic depth, which balances the westward flux difference at the surface.

In contrast to large zonal and upwelling fluxes, the meridional circulation generally transports much smaller fluxes, both within and below the euphotic layer. Between 112 and 252 m, convergent meridional circulation in the west box brings nutrients into the equator, while in the east box meridional fluxes are poleward and stronger. In this depth range, the meridional fluxes of both nutrients in the east box are relatively high, carrying about 35–40% of the EUC nutrient inputs at 135°W and most of them are southward to join the Peru–Chile undercurrent as noted by Toggweiler and Carson (1995). This explains the broader high nutrient band at 200 m seen from WOA98 data and modeled results (not shown). The net difference of meridional fluxes between 112 and 252 m in the Wyrtki box is quite small with 0.7×10^4 mol s^{-1} more NO_3 than $Si(OH)_4$.

Upwelling, including vertical mixing, supplies more NO_3 than $Si(OH)_4$ to the euphotic zone (0–112 m) in the Wyrtki box (37.3×10^4 vs. 31.8×10^4 mol s^{-1}), corresponding to daily mean

Table 3
Annual mean of variables in the CEP and EEP

Variables	West box	East box	Wyrtki box	Matching box[a]	Observations
NO_3 upwelling (120 m, mmol m^{-2} day^{-1})	3.10	2.80	2.95	2.37[b]	2.6[1]
$Si(OH)_4$ upwelling (120 m, mmol m^{-2} day^{-1})	2.50	2.53	2.51	1.96[b]	2.1[1]
NO_3 uptake (0–120 m integrated) (mmol m^{-2} day^{-1})	2.23	2.44	2.33	2.46	2.0[2], 1.56–2.68[3]
$Si(OH)_4$ uptake (0–120 m integrated) (mmol m^{-2} day^{-1})	2.10	3.36	2.73	1.30, 3.30, 0.91	0.8–2.1[4], 3.9[4], 1.78[5]
NO_3 related export production at 120 m (mmol m^{-2} day^{-1})	1.42	1.76	1.59	1.65, 1.72	1.56[6], 0.48[7]
Si related export production at 120 m (mmol m^{-2} day^{-1})	1.16	2.33	1.74	2.0	1.94[8]
Total small phytoplankton biomass (mmol m^{-2})	8.1	7.6	7.9		
Total diatom biomass (mmol m^{-2})	4.0	7.74	5.8		
Mean NO_3 surface/mean/120 m (mmol m^{-3})	4.8/6.0/8.4	6.4/12.5/19			3.75/4.8/6.5(CEP)[9] 5.6/13.2/21.8(EEP)[9]
Mean $Si(OH)_4$ surface/mean/120 m (mmol m^{-3})	2.5/3.4/5.3	3.9/9.8/16.9			2.7/3.0/4.2(CEP)[9] 4.1/9.7/16.1(EEP)[9]
Mean f-ratio	0.28	0.34	0.31		0.1–0.21[c]

[a] These numbers are computed using regions and periods as close to observations as possible. Because this is a climatological modeling, however, the variability with interannual or longer time scale is not taken into account.

[b] Net upwelling, i.e., upwelling excluding horizontal advection fluxes. Zonal flux has large gradient here that cannot be ignored.

[c] Various sources, 0.1–0.17 (McCarthy et al., 1996, synthesis of WEC88 and EqPac I & II), 0.13–0.21 (Raimbault et al., 1999; OLIPAC cruise along 150°W during November, 1994)

[1] Ku et al., 1995, Data: Jan. 29–March 13, 1992 (9°N–12°S, 140°W), weak El Niño

[2] MCarthy et al., 1996, Data: Aug.–Sept. 1992 (5°N–7°S, 140°W).

[3] Raimbault et al., 1999, Data: Nov. 1994, (1°N–5.5°S, 150°W), weak El Niño

[4] Blain et al., 1997, Data: Sept.–Oct. 1994, (a) (0, 165°E–170°W), (b) (0, 170–150°W).

[5] Leynaert et al., 2001, Nov. 1996 (1°N–1°S, 180°W), Neutral Condition

[6] Murray et al., 1996, Data: Aug.–Sept. 1992, (5°N–5°S, 140°W)

[7] Zhang and Quay, 1997, Data: Feb.–May, 1992, EUZ band (2°N–2°S, 170–110°W)

[8] Dunne et al., 1999, Data: Sept.–Oct. 1992, (2°N–2S, 140°W). Rough estimate from numbers on Fig. 4b.

[9] Conkright et al., 1998, WOA98.

values of 2.95 and 2.51 mmol m^{-2} day^{-1}, respectively (Table 3). The nitrate flux is close to the averaged flux of 2.6 mmol m^{-2} day^{-1} measured between 9°N and 12°S along 140°W during the JGOFS EqPac Survey I (Ku et al., 1995), which was estimated by assuming balanced horizontal fluxes. Nonetheless, horizontal flux may not be negligible when dealing with a small zonal area because the shoaling of the EUC core would result in a zonal gradient of flux. For example, computing over box 9°N–12°S, 150–130°W in January–March, we obtained a NO_3 upwelling flux of 6.27×10^4 mol s^{-1}. After excluding the horizontal fluxes, however, the "net upwelling" is 3.57×10^4 mol s^{-1}, which is only 64% of the upwelling flux and equivalent to a daily flux of 2.30 mmol m^{-2} day^{-1}. Therefore the measured estimate is comparatively high if we take into account that EqPac Survey I was carried out during springtime 1992 under a weak El Niño conditions. The $Si(OH)_4$ supply in our model is close to Dugdale and Wilkerson's (1998) box model estimation but higher than 1-D model result (Chai et al., 2002). In comparison, the modeled NO_3 supply is in the middle of the other two model results but much smaller than Toggweiler and Carson (1995) prediction. The ratio of $Si(OH)_4/NO_3$ in the upwelling water is 0.85 (Table 5), which is consistent with the regression slope between 100 and 300 m (see above), but slightly higher than the 0.8 Si/N ratio estimated by Ku et al. (1995).

Within the EUZ, there are two major pathways for nutrient transport (Fig. 6). The majority of fluxes are carried by the EUC to the EEP, where it upwells to the mixed layer or turns south to join the Peru–Chile undercurrent (Toggweiler and Carson, 1995). Part of the upwelling waters is taken up by phytoplankton, and the rest diverges and then is carried westward mainly through the southern branch of the SEC. The other pathway is associated with meridional circulation cells in the CEP, which upwell nutrient near the equator and downwell beyond the EUZ. The biological uptake consumes part of this flux as well. These two pathways are closed by the equatorward flow below the mixed layer in the CEP along with regeneration contributions (Fig. 7). The strong

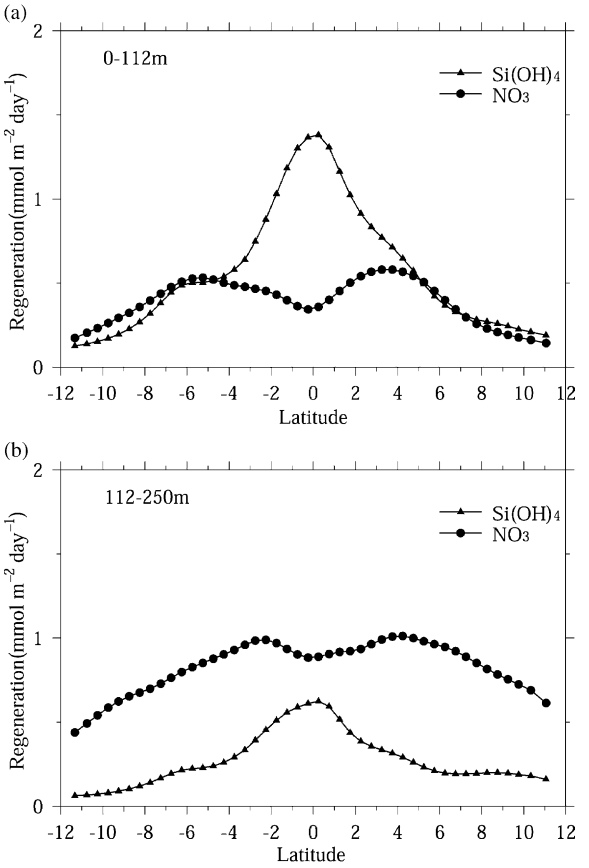

Fig. 7. Zonal averaged nutrient regeneration (nitrification and silicon dissolution) within (a) the upper 112 m (b) and the 112–250 m.

meridional fluxes at the boundaries of EUZ contrast to the low meridional fluxes observed at 5°N and 5°S. This is a dramatic manifestation of the strong latitudinal gradients of circulation, owing to the strong shear between several currents (Fig. 1). Apparently, the system is recycling less $Si(OH)_4$ than NO_3, although the $Si(OH)_4$ uptake in the EEP is higher than that for NO_3 (Table 3, Fig. 5) (see discussion in Section 4.1).

3.4.2. *Nutrient uptake, regeneration and export*

Total NO_3 and $Si(OH)_4$ uptakes within the euphotic zone are 29.5×10^4 and 34.4×10^4 mol s^{-1} (Fig. 5, upper left corners), corresponding to daily mean uptakes of 2.33 and 2.72 mmol m^{-2} day^{-1}, respectively. NO_3 uptake

is in good agreement with the 2.0 mmol m^{-2} day^{-1} from EqPac Survey II measurements (McCarthy et al., 1996), while $Si(OH)_4$ uptake is between the lower limit (0.8–2.1 mmol m^{-2} day^{-1}) of an oligotrophic area (166°E–170°W) and upper limit (3.9 mmol m^{-2} day^{-1}) in a HNLC area (170–150°W) measured during FLUPac (Blain et al., 1997). Even though our west box covers the entire FLUPAC area (170–150°W), $Si(OH)_4$ uptake in this area is significantly lower than the measured results but in the range of oligotrophic results of FLUPAC (Blain et al., 1997). When computing the $Si(OH)_4$ uptake for the specific periods and areas of the measurements, the model gives good comparisons with FLUPAC results (Blain et al., 1997), but the number at 180°W is 0.91 mmol m^{-2} day^{-1}, about half of the 1.78 mmol m^{-2} day^{-1} measured in Nov. 1996 (Leynaert et al., 2001) (Table 3). As noted in Section 2, this is possibly due to the lower Si/N uptake by diatom. However, modeled $Si(OH)_4$ concentration in this area is lower than WOA98 (Figs. 3 and 9). Increasing the Si/N uptake ratio by diatom will drive the system to an even lower $Si(OH)_4$ condition and further deviate from observations. Therefore, a higher BSi dissolution needs to be used if we want to maintain diatom production (this means higher BSi production with higher Si/N uptake ratio). Contrasting to the 0.85:1 Si/N ratio in upwelling areas, the silicate and nitrate are actually taken up on a 1.2:1 ratio, with more silicate than nitrate being taken up in the EEP (Table 5). It is worth to note that since both BSi dissolution and nitrification recycle considerable portions of nutrient uptakes within the euphotic zone, the nutrient uptakes reported here represent the gross uptake only. After excluding the regeneration contribution, the net $Si(OH)_4$ and NO_3 uptake are nearly equal to each other.

As shown in Fig. 5 (lower left corner in each box) and Fig. 7, a majority of NO_3 regeneration occurs below the euphotic depth, while the BSi dissolution mainly occurs in the upper 100 m and decreases rapidly with depth along with the decrease of water temperature. It should be noted that BSi dissolution is also affected by biological processes, in particular bacterial activities (Bidle and Azam, 1999). Therefore, the profile within upper 100 m may be different from those in real cases. The nitrate regeneration rate varies from 2×10^{-3} to 7×10^{-3} mmol m^{-3} day^{-1}, which is lower than, but comparable to, the 10–40 $\times$ 10^{-3} mmol m^{-3} day^{-1} measured between 0° and 10°S at 180°W during OLIPAC (Raimbault et al., 1999). Even at latitudes 10°N or 10°S where the surface nutrient concentration is nearly 0, there is considerable NO_3 regeneration below the euphotic depth (Fig. 7), which could be very important to support the phytoplankton growth at the base of the euphotic layer. Total nitrification within the upper 412 m is 23.7×10^4 mol s^{-1}, accounting for about 80% of the total NO_3 uptake within the euphotic zone (Table 4). This is consistent with the general notion that most of the nitrogen regeneration is done within the upper 400 m (Raimbault et al., 1999). In comparison, the Si dissolution only recycles about 60% of $Si(OH)_4$ uptake in the upper 400 m. On average, dissolution within the euphotic zone contributes to 43% silicate uptake in the central and 30% in the east, comparable to various ratios reported for the world ocean (see Table 1 in Nelson et al., 1995).

The map of biogenic export production at 120 m is quite different from that of organic nitrogen (Fig. 8). The BSi export occurs primarily

Table 4
The percentages of nutrient regeneration in nutrient uptake and export production

	CEP	EEP	Wyrtki box
Dissolution between 0 and 112 m / $Si(OH)_4$ uptake	0.43	0.30	0.35
Nitrification between 0 and 112 m / NO_3 uptake	0.26	0.16	0.21
Dissolution between 112 and 412 m / BSi export at 112 m	0.33	0.40	0.38
Nitrification between 112 and 412 m / Organic nitrogen export at 112 m	0.81	0.92	0.87
Dissolution between 0 and 412 m / $Si(OH)_4$ uptake	0.61	0.58	0.59
Nitrification between 0 and 412 m / NO_3 uptake	0.78	0.82	0.80

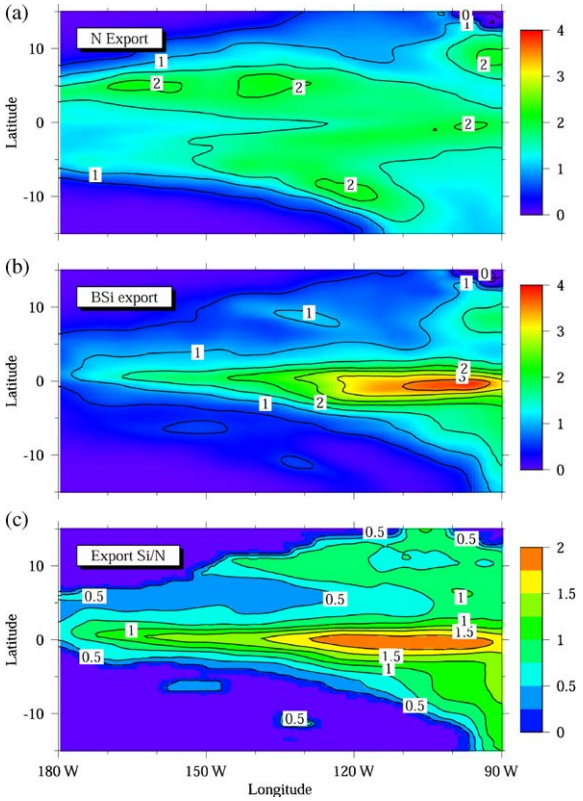

Fig. 8. Annual mean export production at 120 m: (a) organic nitrogen (mmol m^{-2} day^{-1}); (b) BSi (mmol m^{-2} day^{-1}); and (c) Si/N ratio of the export production.

in the EUZ, within which the EEP export is up to 4 mmol m^{-2} day^{-1}, about 3-fold that of the CEP. In contrast, the organic nitrogen export has a much broader tongue and is distributed quite uniformly over the equatorial Pacific. These results are consistent with the 1-D CoSINE results, which showed that Si export responded strongly and positively to increased $Si(OH)_4$ input while organic nitrogen export remained relatively constant (Chai et al., 2002; Dugdale et al., 2002b). Also in agreement with the 1-D model results, Si/N ratios in export are distinctly different between the EUZ and beyond. From Fig. 5, the silica export production within the Wyrtki box can be calculated as 22×10^4 mol s^{-1}, about 64% of the $Si(OH)_4$ uptake, compared to the 20.1×10^4 mol s^{-1} nitrogen export production, which is about 68% of the nitrogen related new production. These give daily mean export production for

Table 5
The molar Si/N ratios in various processes

	West box	East box	Wyrtki box
Uptake	0.94	1.38	1.17
Upwelling supplies	0.81	0.90	0.85
Export production	0.81	1.32	1.09

organic nitrogen and silicon as 1.59 and 1.74 mmol m^{-2} day^{-1}, respectively (Table 3). These numbers compare well with the EqPac Survey II estimates (Dunne et al., 1999) (see Table 3) but are much higher than estimates for the EUZ (2°N–2°S, 170–110°W) under the El Niño condition of 1992 (Zhang and Quay, 1997). The annual Si export within the Wyrtki box is about 11.4 Tmol yr^{-1}, which is in line with estimates of 11.1 and 13.9 Tmol yr^{-1} by Gnanadesikan (1999) for the equatorial Pacific using isopycnal mixing schemes and temperature dependent dissolution in an abiotic global model. The Si and N export to below euphotic zone follows a 0.8:1 ratio in the CEP, compared to a much higher 1.32:1 ratio in the EEP (Table 5), which is mainly due to more BSi production in the east.

4. Discussion

4.1. Why is the nitrate concentration higher than silicate in the equatorial Pacific?

Two major factors contribute to the lower $Si(OH)_4$ than NO_3 supply to the euphotic zone and the maintenance of the less than 1 (0.71) Si/N ratio within the euphotic layer (see Table 3, 6.6/9.25). These are the higher NO_3 than $Si(OH)_4$ flux from the EUC and more efficient recycling of nitrogen than silicon. Observations show that the EUC primarily comes from the NECC and the New Guinea Coastal Undercurrent (NGCUC) (Dugdale et al., 2002b; Toggweiler and Carson, 1995). By analyzing WEPOCS III data acquired during June–July 1988, Dugdale et al. (2002b) showed that NGCUC water has significantly lower $Si(OH)_4$ concentration than NO_3, while the NECC carries slightly higher $Si(OH)_4$ than NO_3. By incorporating model transport with nutrient data,

they further showed that these two flows transport nearly the same amount of water volume, leading to a higher NO_3 than $Si(OH)_4$ input to the EUC at 160°E. While current work focuses on the CEP and EEP and is largely based on model calculations, the fluxes at 180°W also show that the EUC carries more nitrate (31.9×10^4 mol s^{-1}) than silicate (30.3×10^4 mol s^{-1}) across the dateline (Table 6, Fig. 6). The total nutrient flux of EUC follows a 1:1.1 Si/N ratio with a net difference of 1.6×10^4 mol s^{-1}. Computing over a slightly smaller area (2°N–2°S) yields a larger difference 2.2×10^4 mol s^{-1}. It is not clear whether the lower silicate concentrations in the Peru upwelling system contribute to the lower silicate concentration south of the equator via the SEC. The model indeed shows a higher nitrate than silicate influx at 90°W between 0°S and 5°S within the upper 50 m. However, the modeled low production in the Peru upwelling system may not be realistic because the model is not suitable to resolve the coastal upwelling in this area.

Another important factor to the imbalance of nutrient sources is the more efficient recycling of nitrogen than silicon (Table 4). About 38% of the BSi export production is remineralized within 300 m below the euphotic layer. In contrast, about 87% of the export production of nitrogen is recycled within this 300 m range. Faster sinking velocity of siliceous particles makes them relatively unavailable for dissolution to take place in the top layer. Furthermore, a higher than 1 Si/N uptake ratio by diatoms allows for more silicate removal than nitrogen. Once BSi sinks out of the euphotic zone, the dissolution of BSi is further reduced because of the rapid decrease of temperature. It is interesting to see that the contribution of nitrification in the EUZ is lower than $Si(OH)_4$ (Table 6). This is reasonable if we consider that most silicate uptake occurs in this 2.5°N–2.5°S band, while more small phytoplankton growth is taking place beyond the EUZ. The faster nitrogen regeneration actually contributes to the much higher meridional NO_3 inflow (see Table 6). A budget calculation in the box 2.5–10°N, 180–90°W, 50–252 m, for example, shows the nitrate regeneration is 6.2×10^4 mol s^{-1} higher than silicate regeneration (Table 7). Excluding the south face of this box, the total advection contributes 1.0×10^4 mol s^{-1} more NO_3 than $Si(OH)_4$ inflow. This illustrates that the regeneration difference in this box contributes to most of the higher NO_3 than $Si(OH)_4$ subsurface flux at 2.5°N. At 2.5°S, the subsurface inflow in the CEP is partly compensated by the outflow in the EEP. The difference

Table 6
Nutrient fluxes to the upper layer of central and eastern equatorial upwelling zone (2.5°N–2.5°S, 180–90°W)[a] (10^4 mol s^{-1})

Sources	NO_3	$Si(OH)_4$
EUC (50–252 m)	31.9	30.3
Regeneration (0–252 m)	8.9	11.2
Upwelling at 252 m	11.0	11.4
North inflow (50–252 m)	10.2	3.4
South inflow (50–252 m)	1.2	−4.7[b]

[a] All major sources are counted in this table, therefore the outflow of SEC and meridional divergence on the top layer are not included. The nitrification is calculated throughout the top 252 m. The meridional fluxes have dramatic differences, which mainly occur between 40 and 140 m.

[b] Negative means that flux is out of the box.

Table 7
The inflow differences of NO_3 and $Si(OH)_4$ between 50 and 252 m on both sides of EUC (2.5°N and 2.5°S) and the regeneration contributions[a]

	180–135°W Remin./total diff.	135–90°W Remin. /total diff.[b]	180–90°W Remin./total diff.
North face (2.5°N)	3.1/5.4	2.8/1.5	5.9/6.9
South face (2.5°S)	2.7/6.9	2.5/−0.9	5.2/6.0

[a] The remineralizations of nutrients were computed over a box attaching to each side with latitudinal ranges (2.5–10°N) for north face and (2.5–10°S) for south face, respectively.

[b] All flows are poleward but nitrate has less flux at north face (positive difference) or more flux at south face (negative difference).

of NO_3 and $Si(OH)_4$ influxes in the CEP (180–135°W, 50–252 m) is 6.7×10^4 mol s^{-1} with 41% coming from local regeneration difference and the rest from advection difference. In other words, much more nitrogen regeneration than Si dissolution takes place beyond the EUZ and then re-circulates back to the equator, particularly in the CEP. As noted in Section 3.4.1, the meridional circulation cells in the CEP, in association with nitrogen regeneration, effectively re-circulate nitrogen back to equatorial upwelling. Based on the measurements in OLIPAC, Raimbault et al. (1999) speculated that this mechanism is a "very efficient system for recycling inorganic nitrogen in the euphotic layer and thus for supporting the high regenerated production levels". Another pathway of nutrient cycling is the transport to the EEP by the EUC, where nutrients are upwelled to the euphotic layer and then directed to the CEP via equatorial divergence and the SEC (Fig. 6). Again, local biological uptake and regeneration occur along with this path. It appears that BSi does not participate significantly in these two recycling systems because the BSi production mainly occurs within the EUZ and BSi sinks relatively faster. Taken together, the higher $Si(OH)_4$ than NO_3 (Table 3, Fig. 5) and lower silicate regeneration than nitrate suggest a much slower recycling of silicon than nitrogen.

It should be noted that the relative efficiency of nitrogen and silicon recycling is sensitive to parameterization of the remineralization of organic materials and biogenic silica, in which many biochemical processes are involved and not well quantified. In particular, the Si/N uptake ratio, the sinking velocity of particles, the maximum dissolution rate of BSi at the surface and the slope of the Martin function (Martin et al., 1987) are critical parameters. In the current simulation, we believe the estimate of BSi dissolution is on the higher end since we use a relatively high value of dissolution rate (0.2 day^{-1}) and a median sinking velocity (20 m day^{-1}) of BSi, as compared to 50 m day^{-1} or higher used in other models (e.g., Gnanadesikan, 1999). The sole temperature dependence of BSi dissolution used in the current simulation does not incorporate many other factors such as particle size and ambient $Si(OH)_4$ concentration. In particular, dissolution rate has a maximum at the surface because the temperature in this area usually decreases with depth. This is opposite to the observed profiles in euphotic zone. For example, Nelson and Goering (1977) showed that specific dissolution of BSi increases from nearly zero at the surface to more than 0.5 day^{-1} at 50 m in an upwelling region off northwest Africa. The possible reason for this is the low bacterial activities due to light inhibition such that the organic coating is barely removed to expose the biogenic frustules. Unlike previously thought, the bacterial attack on the organic surface will accelerate the dissolution (Bidle and Azam, 1999). Therefore, this formulation may overestimate the dissolution rate near the surface. However, due to strong upwelling and wind mixing in the euphotic zone, this should not have significant influences on the Si cycling in the equatorial band. Moreover, the Si/N uptake ratio of 1.5 is clearly one of the lowest values reported so far for iron-limitation conditions. As a result, the model may underestimate BSi production and thus BSi export production, which may be the reason for lower than observed BSi production in the CEP (Table 3). This may over-predict the silicon recycling efficiency as well. As noted in Section 3.4.2, one way to mitigate this problem is increasing the Si/N ratio while increasing the BSi dissolution rate as well. These will be tested in the future. On the other hand, the power index of the Martin function (Martin et al., 1987) for nitrogen regeneration is 0.72, which is in a midpoint of 0.6–0.81 reported from recent synthesis by Berelson (2001) for the equatorial Pacific and is much lower than the 0.858 originally suggested by Martin et al. (1987). In summary, the current prediction of BSi dissolution is on the high end while nitrogen regeneration is on the low end or median end. Therefore, it is likely that relatively high nitrogen recycling predicted here is still a conservative estimate.

4.2. The role of silicate conditions on the new production

There are several important differences between the west and east boxes in Fig. 5; all of which are

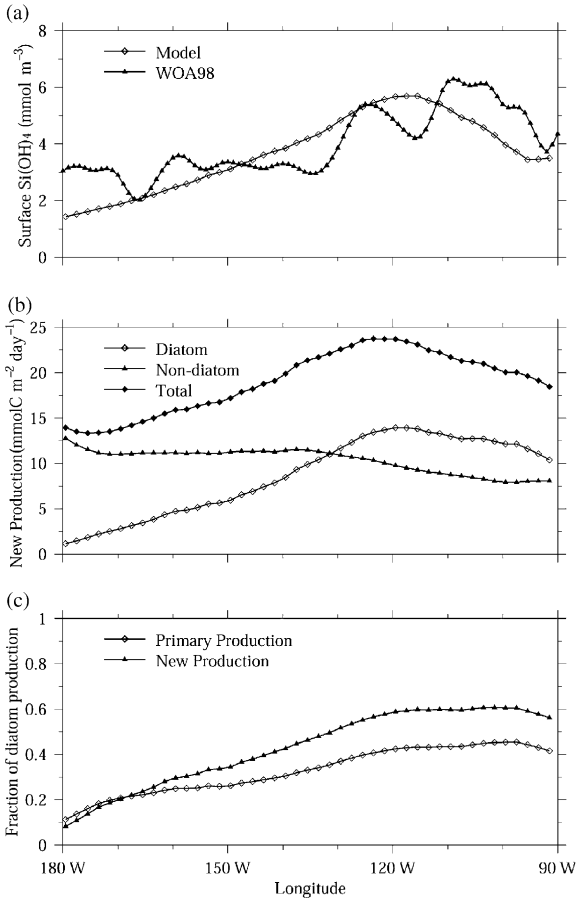

Fig. 9. $Si(OH)_4$ concentrations and new production averaged over 2°N–2°S: (a) modeled and observed (WOA98) surface silicate concentration; (b) diatom, non-diatom and total new production; and (c) fractions of diatom contributions to the new production and primary production.

closely related to $Si(OH)_4$ concentrations. The diatom biomass nearly doubles in the east associated with much higher silicate support at 120 m and the resulting high surface $Si(OH)_4$ concentration (Table 3, Fig. 9a). As a result, the BSi production and export in the east is nearly double that of the west box. In contrast, the non-diatom new production decreases slightly to the east (Fig. 9b), in agreement with 1-D experiments that showed non-diatom activity decreasing with increasing diatom proportion of the phytoplankton (Dugdale et al., 2002a). The total new production closely follows the variability of surface $Si(OH)_4$ as well (Fig. 9b). The contribution of diatoms to the total new production averaged over 2°N–2°S increases almost linearly from about 10% at the dateline to more than 60% east of 130°W (Fig. 9c). The contribution of diatom related primary production has similar linear trend but less in percentage, increasing from 12% at the dateline to about 45% in the east. East of 130°W, surface $Si(OH)_4$ concentration is higher than 3.5 mmol m^{-3}, and the percentages of diatom contribution to both the new and primary production remain largely unchanged, contrasting to the considerable variations of silicate in both the observation and model. West of 140°W, the gradient of diatom production may be overestimated since the stepwise feature of silicate concentration was not reproduced in the model. A detailed partition of the new production due to small phytoplankton and diatoms shows that small phytoplankton at 160°W predominantly contributes to the new production and most of the diatom production occurs within a narrow band between 2°N and 1°S (Fig. 10a). In comparison, the diatom production dominates the new production in an area (1°N–2°S) at 110°W (Fig. 10b). Beyond the EUZ, diatoms tend to sink out of the euphotic layer rapidly because of low upwelling or downwelling of waters. At low $Si(OH)_4$ concentrations outside the EUZ, diatom growth is unable to offset losses, including sinking. Enclosure experiments (Egge and Aksnes, 1992) showed diatoms do poorly and lose out to other phytoplankton at $Si(OH)_4$ concentrations less than 2 mmol m^{-3}, and our model results are consistent with these experimental data. Evidence for decline in diatom activity is that the 1 mmol m^{-3} silicate isopleth can extend further south than nitrate, even though silicate concentration on the equator is much lower than nitrate, which can be seen in both the model and observations (Fig. 2).

The close correlation of the diatom new production and total new production with surface $Si(OH)_4$ concentration shown in Fig. 9 suggests that the silicate condition plays a key role in the zonal variability of phytoplankton new production. The Si limitation of diatom growth in the CEP is evident from the low specific diatom growth rate (0.2–0.6 day^{-1}) along 160°W (not

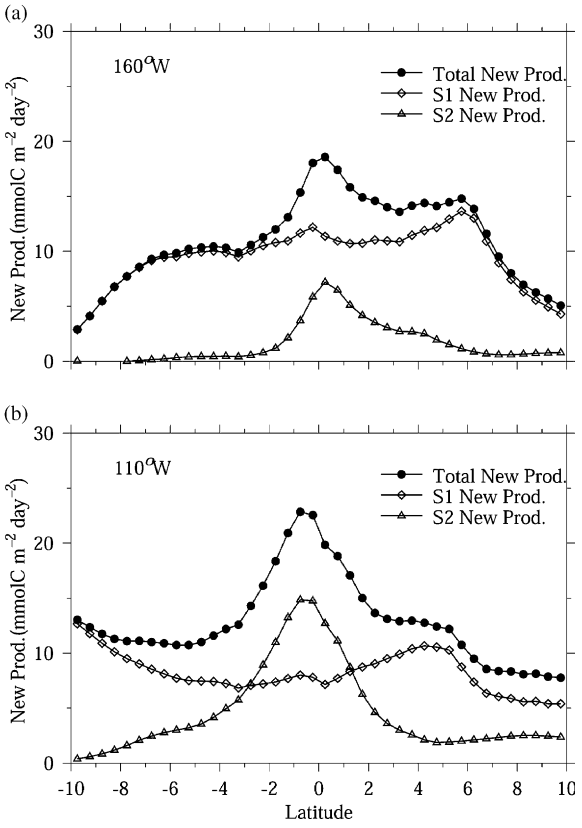

Fig. 10. Partitions of new production by diatom (S2) and non-diatom (S1) at (a) 160°W and (b) 110°W.

shown), which is much lower than the maximal diatom growth rate (2.0 day^{-1}). By performing kinetics experiments of $Si(OH)_4$ uptake, Leynaert et al. (2001) showed that in situ uptake rates of diatoms at 1°N–1°S, 180°W were restricted to 13–78% of the maximum diatom uptake rate, dependent on the ambient silicate concentration. The Leynaert et al. (2001) results confirm the regulation of diatom processes by $Si(OH)_4$ in the EUZ, with diatom growth rate and $Si(OH)_4$ concentrations set by loss rates, primarily grazing (Dugdale et al., 2002a). The $Si(OH)_4$ source concentration in the EEP is relatively high and therefore allows more diatom growth potentially. The result is that diatom production dominates the new production, as noted above, and the specific growth rate of diatoms increases with maximal value at the equator reaching 1.1 day^{-1}, despite the same iron stress (low α_{max}) being applied. The non-diatom related new production slightly decreases to the east, an indication of diatom and therefore Si regulation as well. As a result, the total new production is closely correlated with ambient silicate concentration as well, with low production in the CEP and high production in the EEP (Fig. 9b).

The increase in the percentage of diatom new production to the east suggests a possible tighter nitrogen and silicon coupling in the EEP, compared to the CEP. The ratio of silicate and nitrate uptake in the east box is about 1.38:1 compared to 0.94 in the west box, and the export Si/N ratio is 1.32 in the east versus 0.81 in the west box. Using the 1-D CoSINE model, Dugdale et al. (2002a) conducted 1-D numerical experiments and tested the sensitivity of diatom production to variations of silicate concentrations in the source waters. The results showed that the proportion of new production carried out by diatoms increases quasi-linearly from less than 0.1 at the lowest silicate source concentration (3.0 mmol m^{-3}) to nearly 0.8 at the highest (15.0 mmol m^{-3}) silicate source concentration, closely resembling the change in source silicate concentrations and resulting fraction of production from the CEP to the EEP in the current model (Table 3, Figs. 9 and 10). By examining the Si/N ratios in sediment trap and nutrient concentrations, Dunne et al. (1999) argued that silicon and nitrogen are tightly coupled only at periods of high nutrient concentrations and non-steady state. Our results are conceptually consistent with this argument while derived from relatively stable conditions.

The effects of low Si conditions in the CEP can be further explored in two ways (Table 8, Fig. 11). First, we increase the Si concentration in this area by artificially reducing the Si/N uptake ratio of diatoms to 0.5:1 (case 1). As expected, the numerical experiment shows that averaged diatom new production in the CEP (2°N–2°S, 180–135°W) almost triples and total new production increases 26%, along with the increase of Si concentration from about 2.4 mmol m^{-3} to more than 4 mmol m^{-3}, while the non-diatom new production decreased about 20% (Table 8). It is interesting to see that both the diatom and total

Table 8
Comparisons of different variables in the CEP and EEP for three numerical experiments

	CEP (2°N–2°S, 180–135°W)			EEP (2°N–2°S, 135–90°W)		
	Control	Case 1 (Si/N = 0.5)	Case 2 (50%α_{max})	Control	Case 1 (Si/N = 0.5)	Case 2 (50%α_{max})
Surface $Si(OH)_4$ (mmol m^{-3})	2.3	4.6	3.6	4.4	6.3	6.4
Surface NO_3 (mmol m^{-3})	4.6	5.6	6.6	6.4	7.6	8.7
Non-diatom new prod. (mmol C m^{-2} day^{-1})	10.2	7.9 (−20%)[a]	4.9 (−52%)	8.4	7.1 (−16%)	3.6 (−57%)
Diatom new prod. (mmol C m^{-2} day^{-1})	3.5	9.4 (168%)	5.2 (48%)	11.2	14.8 (32%)	7.8 (−30%)
Total new prod. (mmol C m^{-2} day^{-1})	13.7	17.3 (26%)	10.1 (−26%)	19.7	21.9 (11%)	11.4 (−42%)

[a] The numbers in parentheses are percentages of changes relative to control case.

new production in the EEP increase about 32% and 11%, respectively. This suggests that the potential maximum of new production could be set by the α_{max} and has not been reached yet. Second, we imposed stricter iron limitation on the photosynthesis by reducing the value of α_{max} by half while keeping other parameters unchanged (case 2). Not surprisingly, the non-diatom and total new production in both the CEP and EEP decreases by roughly half and one-third, respectively. However, the averaged diatom new production in the CEP increases about 48%, whereas it reduces 30% in the EEP (Table 8). The higher diatom production in the CEP, compared to control case, is clearly due to higher $Si(OH)_4$ concentrations, which is a result of westward transport of excessive silicate in the east. This reveals the complex interaction between the CEP and EEP under variable conditions of Fe and $Si(OH)_4$. The results of these two numerical experiments demonstrated that $Si(OH)_4$ in the CEP is limiting diatom growth with the current α_{max}, and higher $Si(OH)_4$ concentration will support higher diatom production and total new production, whereas the high $Si(OH)_4$ supply in the EEP could potentially drive that area into Fe limitation.

The current model results suggest a possible zonal gradient for chlorophyll and new production in the equatorial Pacific. Diatoms can grow fast under favorable conditions in this area, and changes in $Si(OH)_4$ source concentrations and $Si(OH)_4$ flux may account for most of the zonal variability in new production. For example, a significant diatom bloom was observed along the great front at 2°N during EqPac Survey II (Archer et al., 1997). Strutton and Chavez (2000) also observed about a 3-fold increase of Chl *a* contribution by > 5 μm phytoplankton group from El Niño to La Niña conditions in 1997–1998. Most observations and modeling results seem to support the view of a zonal gradient. The observations of EqPac Survey II (see Fig. 6 in Chavez et al., 1996) show that the fraction of Chl *a* in particle size > 5 μm (presumably diatom) doubled from west of 140°W to 130–90°W, though no obvious primary productivity increase was observed. Barber and Chavez (1991) summarized the observations from 16 cruises and reported that mean chlorophyll between 5°N and 5°S increases from 15 mg m^{-2} at 160° E to around 20 mg m^{-2} at 150° W (see Fig. 4 in Barber and Chavez (1991)). Their results showed a clear increase of Chl-specific primary productivity along the equator as well. Clear zonal trends also can be readily identified from BSi concentration and silicate uptake rates between 180 and 155°W during FLUPAC (Blain et al., 1997). The results from a sediment model (Heinze et al., 1999) showed a high biogenic Si tongue along the equator originating from the eastern coast, which compares well with historical sediment trap data collected in

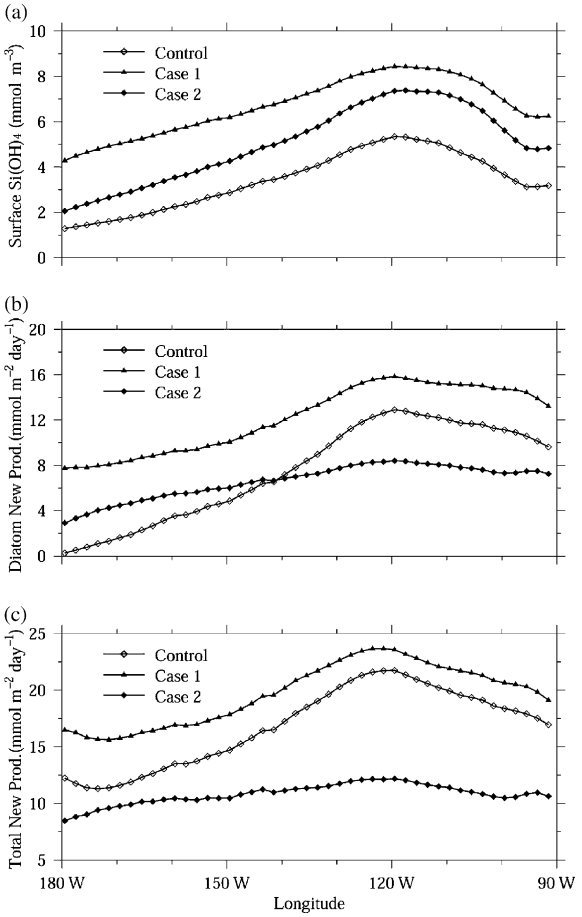

Fig. 11. Comparisons of $Si(OH)_4$, diatom new production, and total new production averaged over 2°N–2°S in three numerical experiments: control, case 1 ($Si/N = 0.5$) and case 2 (50% α_{max}): (a) $Si(OH)_4$; (b) diatom new production; and (c) total new production.

this area. Examining the Zonal Flux Cruise data along the equator, however, Le Borgne et al. (1999) did not find a significant zonal trend for either of the planktonic biomass or carbon flux. Nevertheless, this does not rule out the possible existence of a zonal trend for Si-related biological parameters.

4.3. The roles of iron limitation

Iron limitation is implicitly included in the biological model (Chai et al., 2002). The similar approach was used in the 3-D ecosystem modeling study by Chai et al. (1996, 1999) for the equatorial Pacific Ocean to address iron limitation and microzooplankton grazing. The low initial slope (α_{max}) of the *P–I* curve represents a mean low iron condition, which is consistent with the concept of climatological modeling. This may affect the model prediction in several aspects: (a) In areas with relatively high silicate, such as the far eastern equator, iron limitation may become more important; therefore, the current model may over-estimate the production if the α_{max} is too high. In the CEP, it is hard to evaluate whether Fe or $Si(OH)_4$ is limiting since both $Si(OH)_4$ and Fe concentrations are low. If both are limiting or Si is limiting, then a fixed low α_{max} will not affect the result. If the Fe stress is stronger, then the model may over-estimate the production. Based on the comparison of modeled production with observed production (Fig. 4), it seems the α_{max} in the current model is low enough to account for potential iron limitation. (b) There is no direct linkage between the Fe and Si/N uptake ratio of diatoms in the model. Note that the current Si/N ratio is a low value compared to Si/N ranges from field experiments (Takeda, 1998; Franck et al., 2000). The low BSi production predicted may be due to a low Si/N uptake ratio. While low iron possibly will reduce the carbon production, a higher Si/N uptake ratio will compensate the $Si(OH)_4$ uptake and therefore bring $Si(OH)_4$ concentrations lower. In order for the $Si(OH)_4$ concentrations predicted to not deviate from climatological data, a higher Si/N will need higher dissolution compensation, which may not be realistic since current maximal dissolution at the surface is already a high value of 0.2 day^{-1} at 25° C. (c) A constant α_{max} will certainly reduce the temporal and spatial variability of phytoplankton biomass and production when light and other nutrient support are sufficient for phytoplankton growth, but with variable supply of Fe. In particular, this may reduce the latitudinal gradient of production because the equatorial upwelling usually has higher iron supplies such that α_{max} has a local maximum near the equator (Lindley et al., 1995). However, this should not cause substantial impacts on the mean results within the equatorial band in the current climatological modeling.

The possible role of Si regulation on the new production can be viewed as a modification to the conceptual model by Landry et al. (1997), which combines the iron limitation to the diatom growth and microzooplankton grazing control on the small phytoplankton. Consistent with Landry et al. (1997), the small phytoplankton in the current model dominate the primary production and are held nearly constant by microzooplankton grazing (Table 3). The grazing of mesozooplankton only consumes a small fraction (13%) of primary production, compared to 15% during EqPac Survey I and 19.5% during EqPac Survey II (Landry et al., 1997). While we are unable to test the concept that diatoms may escape grazing under favorable conditions in the current framework of climatological modeling, our relatively high diatom production in the east seems to be consistent with this possibility. The key modifications from our results are two-fold. First, the diatom production in the equatorial Pacific could be higher with sufficient silicate even under relatively stable conditions. Second, low silicate in the CEP may co-limit the diatom production while iron limitation sets the upper limit of new and primary production. This also suggests that iron limitation determines the total biomass, while the availability of silicate concentration changes the phytoplankton assemblage and also controls the export production of biogenic silicon, consistent with the silicon pump concept (Dugdale et al., 1995; Dugdale and Wilkerson, 1998; Tréguer and Pondaven, 2000).

5. Summary

A budget calculation of NO_3 and $Si(OH)_4$ in the central equatorial Pacific (CEP) and eastern equatorial Pacific (EEP) was carried out based on a 3-D circulation model and 1-D biogeochemical (CoSINE) model (Chai et al., 2002). Overall, the modeled circulation and nutrient concentrations compare well with the historical observations. The modeled new production in the Wyrtki box compares well with the field measurements and other model estimates, while the modeled primary production is on the lower end of observations (Fig. 4, Table 2). Computed over regions and times similar to the field measurements (ignoring the inter-annual and longer time-scale variability), the modeled upwelling nutrient fluxes, biological uptake rates and organic material exports are in good agreement with observations (Table 3).

The analysis of the NO_3 and $Si(OH)_4$ budgets suggests that nitrogen recycling is faster than that of silicon and is an important addition to the unbalanced NO_3 and $Si(OH)_4$ supplies from the EUC in maintaining a lower than 1 Si/N ratio in the CEP and EEP. The meridional recirculation cells, the EUC and the SEC transports combined with faster regeneration makes the equatorial Pacific an efficient recycling system for N. However, the relatively faster sinking velocity of BSi, higher Si uptake and BSi export in the EUZ makes Si recycling relatively inefficient.

Our model results suggest that diatom growth in the CEP is potentially limited by available silicate, although Fe limitation cannot be ruled out. In association with the relatively higher silicate concentration, diatom related production in the EEP is higher and therefore contributes more to the new, primary and export production. In contrast, the production associated with small phytoplankton is nearly constant along the equator. As a result, the total new production is higher and the Si/N ratio is greater than 1 in the export production in the EEP. Taken together, our model results suggest a potential role for Si regulation on the new production and carbon cycle in this area.

Acknowledgements

This research was supported by NASA and NSF Grants to F. Chai. The model simulations were conducted on the computer at JPL super computing center funded through NASA. Dr. John Dunne and two anonymous reviewers provided comments that greatly improved the final version of the manuscript. This publication is US JGOFS contribution number 864.

References

Archer, D., Aiken, J., et al., 1997. A meeting place of great ocean currents: shipboard observations of a convergent front at 2°N in the Pacific. Deep-Sea Research II 44 (9–10), 1827–1850.

Barber, R.T., Chavez, F.P., 1991. Regulation of primary productivity rate in the equatorial Pacific. Limnology and Oceanography 36 (8), 1803–1815.

Barber, R.T., Sanderson, M.P., Lindley, S.T., et al., 1996. Primary productivity and its regulation in the equatorial Pacific during and following the 1991–1992 El Niño. Deep-Sea Research II 43 (4–6), 933–969.

Berelson, W.M., 2001. The flux of particulate organic carbon into the ocean interior: a comparison of four US JGOFS regional studies. Oceanography 14 (4), 59–67.

Bidle, K.D., Azam, F., 1999. Accelerated dissolution of diatom silica by marine bacterial assemblages. Nature 397, 508–512.

Blain, S., Leynaert, A., Tréguer, P., Chretiennot-Dinet, M., Rodier, M., 1997. Biomass, growth rates and limitation of equatorial Pacific diatoms. Deep-Sea Research I 44 (7), 1255–1275.

Bryden, H.L., Brady, E.C., 1985. Diagnostic model of three-dimensional circulation in the upper equatorial Pacific Ocean. Journal of Physical Oceanography 5, 1255–1273.

Brzezinski, M., 1985. The Si:C:N ratio of marine diatoms: interspecific variability and the effect of some environmental variables. Journal of Phycology 21, 347–357.

Brzezinski, M.A., Nelson, D.N.M., 1995. The annual silica cycle in the Sargasso Sea near Bermuda. Deep-Sea Research I 42 (7), 1215–1237.

Butt, J., Lindstrom, E., 1994. Currents of the east coast of New Ireland, Papua-New Guinea, and their relevance to regional undercurrents in the western equatorial Pacific Ocean. Journal of Geophysical Research 99, 12203–12514.

Carr, M-E., Oakey, N.S., Jones, B., Lewis, M.R., 1992. Hydrographic patterns and vertical mixing in the equatorial Pacific along the 150°W. Journal of Geophysical Research 97, 611–626.

Chai, F., Lindley, S.T., Barber, R.T., 1996. Origin and maintenance of a high nitrate condition in the equatorial Pacific. Deep-Sea Research II 43 (4–6), 1031–1064.

Chai, F., Lindley, S.T., Toggweiler, J.R., Barber, R.T., 1999. Testing the importance of iron and grazing in the maintenance of the high nitrate condition in the Equatorial Pacific Ocean, a physical–biological model study. In: Hanson, R.B., Ducklow, H.W., Field, J.G. (Eds.), The Changing Ocean Carbon Cycle. International Geosphere–Biosphere Programme (IGBP) Book Series 5. Cambridge University Press, London, pp. 156–186.

Chai, F., Dugdale, R.C., Peng, T.-H., Wilkerson, F.P., Barber, R.T., 2002. One dimensional ecosystem model of the equatorial Pacific upwelling system, Part I: model development and silicon and nitrogen cycle. Deep-Sea Research II 49 (13–14), 2713–2745.

Chai, F., Jiang, M.-S., Barber, R.T., Dugdale, R.C., Chao, Y., 2003. Interdecadal variation of the transition zone chlorophyll front: a physical–biological model simulation between 1960 and 1990. Journal of Oceanography 59, 461–475.

Chavez, F.P., Barber, R.T., 1987. An estimate of new production in the equatorial Pacific. Deep-Sea Research 34 (7), 1229–1234.

Chavez, F.P., Toggweiler, J.R., 1995. Physical estimates of global new production: the upwelling contribution. In: Summerhayes, C.P., et al. (Ed.), Upwelling in the Ocean: Modern Processes and Ancient Records. Wiley, New York, pp. 313–320.

Chavez, F.P., Buck, K.R., Service, S.K., Newton, J., Barber, R.T., 1996. Phytoplankton variability in the central and eastern tropical Pacific. Deep-Sea Research II 43 (4–6), 835–870.

Christian, J.R., Verschell, M.A., Murtugudde, R., Busalacchi, A.J., McClain, C.R., 2001. Biogeochemical modeling of the tropical Pacific Ocean. I. Seasonal and interannual variability. Deep-Sea Research II 49 (1–3), 509–543.

Coale, K.H., Johnson, K.S., Fitzwater, S.E., Gordon, R.M., Tanner, S., Hunter, C.N., Chavez, F.P., Ferioli, F.P., Sakamoto, L., Rogers, P., Millero, F., Steinberg, P., Nightingale, P., Cooper, D., Cochlan, W.P., Landry, M.R., Constantinou, J., Rollwagen, G., Trasvina, A., Kudela, R., 1996. A massive phytoplankton bloom induced by an ecosystem-scale iron fertilization experiment in the equatorial Pacific. Nature 383, 495–501.

Conkright, M.E., Levitus, S., Boyer, T.P., 1994. World Ocean Atlas 1994. Vol. 1: Nutrients. NOAA Atlas NESDIS 1. US Department of Commerce, Washington, DC, 150pp.

Conkright, M.E., Levitus, S., O'Brien, T., Boyer, T.P., Stephens, C., Johnson, D., Stathoplos, L., Baranova, O., Antonov, J., Gelfeld, R., Burney, J., Rochester, J., Forgy, C., 1998. World Ocean database 1998, CD-ROM Data Set Documentation, National Oceanographic Data Center Internal Report 14, 111pp.

Cullen, J.J., Lewis, M.R., Davis, C.O., Barber, R.T., 1992. Photosynthetic characteristics and estimated growth rates indicate grazing is the proximate control of primary production in the equatorial Pacific. Journal of Geophysical Research 97, 639–654.

Dore, J.E., Karl, D.A., 1996. Nitrification in the euphotic zone as a source for nitrite, nitrate, and nitrous oxide at Station ALOHA. Limnology and Oceanography 41 (8), 1619–1628.

Dugdale, R.C., Wilkerson, F.P., 1998. Silicate regulation of new production in the equatorial Pacific upwelling. Nature 391, 270–273.

Dugdale, R.C., Wilkerson, F.P., Barber, R.T., Chavez, F.C., 1992. Estimating new production in the Equatorial Pacific Ocean at 150°W. Journal of Geophysical Research 97 (C1), 681–686.

Dugdale, R.C., Wilkerson, F.P., Minas, H.J., 1995. The role of a silicate pump in driving new production. Deep-Sea Research I 42, 697–719.

Dugdale, R.C., Barber, R.T., Chai, F., Peng, T.-H., Wilkerson, F.P., 2002a. One dimensional ecosystem model of the equatorial Pacific upwelling system, Part II: sensitivity

analysis and comparison with JGOFS EqPac data. Deep-Sea Research II 49 (13–14), 2746–2762.

Dugdale, R.C., Wischmeyer, A.G., Wilkerson, F.P., Barber, R.T., Chai, F., Jiang, M.-S., Peng, T.-H., 2002b. Meridional asymmetry of source nutrients to the Equatorial Pacific upwelling ecosystem and its potential impact on Ocean–Atmosphere CO_2 flux: a data and modeling approach. Deep-Sea Research II 49 (13–14), 2713–2732.

Dunne, J.P., Murray, J.W., Aufdenkampe, A.K., Blain, S., Rodier, M., 1999. Silicon–nitrogen coupling in the equatorial Pacific upwelling zone. Global Biogeochemical Cycles 13, 715–726.

Egge, J.K., Aksnes, D.L., 1992. Silicate as regulation nutrient in phytoplankton competition. Marine Ecology Progress Series 83, 281–289.

Eppley, R.W., 1972. Temperature and phytoplankton growth in the sea. Fishery Bulletin 70 (4), 1063–1085.

Franck, V.M., Brzezinksi, M.A., Coale, K.H., Nelson, D.M., 2000. Iron and silicic acid concentrations regulate Si uptake north and south of the Polar Frontal Zone in the Pacific Sector of the Southern Ocean. Deep-Sea Research II 47, 3315–3338.

Frost, B.W., Frenzen, N.C., 1992. Grazing and iron limitation in the phytoplankton stock and nutrient concentration: a chemostat analogue of the Pacific equatorial upwelling zone. Marine Ecology Progress Series 83, 291–303.

Gent, P., McWilliam, J.C., 1990. Isopycnal mixing in ocean circulation models. Journal of Physical Oceanography 20, 150–155.

Gent, P.R., Bryan, F.O., Danabasoglu, G., Doney, S.C., Holland, W.R., Large, W.G., McWilliams, J.C., 1998. The NCAR climate system model global ocean component. Journal of Climate 11 (6), 1287–1306.

Gnanadesikan, A., 1999. A global model of silicon cycling: sensitivity to eddy parameterization and dissolution. Global Biogeochemical Cycles 13 (1), 199–220.

Heinze, C., Maier-Reimer, E., Winguth, A.M.E., Archer, D., 1999. A global oceanic sediment model for long-term climate studies. Global Biogeochemical Cycles 13 (1), 221–250.

Holland, W.R., Chow, J.J.C., Bryan, F.O., 1998. Application of a third-order upwind scheme in the NCAR ocean model. Journal of Climate 11, 1487–1493.

Hutchins, D.A., Bruland, K.W., 1998. Iron-limited diatom growth and Si:N uptake ratios in a coastal upwelling regime. Nature 393, 561–564.

Johnson, G.C., McPhaden, M.J., 1999. Interior pycnocline flow from the subtropical to the equatorial Pacific Ocean. Journal of Physical Oceanography 29, 3073–3089.

Johnson, G.C., McPhaden, M.J., Firing, E., 2001. Equatorial Pacific Ocean horizontal velocity, divergence and upwelling. Journal of Physical Oceanography 31 (3), 839–849.

Ku, T.-L., Luo, S., Kusakabe, M., Bishop, J.K.B., 1995. ^{228}Ra-derived nutrient budgets in the upper equatorial Pacific and the role of "new" silicate in limiting productivity. Deep-Sea Research II 42 (2–3), 479–498.

Landry, M.R., Barber, R.T., Bidigare, R.R., Chai, F., Coale, K.H., Ham, H.G., Lewis, M.R., McCarthy, J.J., Roman, M.R., Stoecker, D.K., Verity, P.G., White, J.R., 1997. Iron and grazing constrains on primary production in the central equatorial Pacific: an EqPac synthesis. Limnology Oceanography 42 (3), 405–418.

Large, W.G., McWilliams, J.C., Doney, S.C., 1994. Oceanic vertical mixing: a review and a model with a nonlocal boundary layer parameterization. Review of Geophysics 32, 363–403.

Le Borgne, R., Rodier, M., Le Bouteiller, A., Murray, J.W., 1999. Zonal variability of plankton and particle export flux in the equatorial Pacific upwelling between 165°E and 150°W. Oceanologica Acta 22 (1), 57–66.

Leonard, C.L., McClain, C.R., Murtugudde, R., Hofmann, E., Harding Jr., L.W., 1999. An iron-based ecosystem model of the central equatorial Pacific. Journal of Geophysical Research 104 (C1), 1325–1341.

Levitus, S., Burgett, R., Boyer, T., 1994. World Ocean Atlas 1994, Vol. 3: Salinity and Vol. 4, Temperature, NOAA Atlas NEDIS 3-4, US Department of Commerce.

Leynaert, A., Treguer, P., Lancelot, C., Rodier, M., 2001. Silicon limitation of biogenic silica production in the Equatorial Pacific. Deep-Sea Research I 48, 639–660.

Li, X.J., Chao, Y., McWilliams, J.C., Fu, L.L., 2001. A comparison of two vertical mixing schemes in a Pacific Ocean General Model. Journal of Climate 14, 1377–1398.

Lindley, S.T., Bidigare, R.R., Barber, R.T., 1995. Phytoplankton photosynthetic parameters along 140°W in the equatorial Pacific. Deep-Sea Research II 42 (2–3), 441–463.

Louanchi, F., Najjar, R.G., 2000. A global monthly climatology of phosphate, nitrate, and silicate in the upper ocean: Spring–summer export production and shallow remineralization. Global Biogeochemical Cycles 14 (3), 957–977.

Lu, P., McCreary Jr., J.P., Klinger, B.A., 1998. Meridional circulation cells and the source waters of the Pacific Equatorial Undercurrent. Journal Physical Oceanography 28, 62–84.

Martin, J.H., 1990. Glacial–interglacial CO_2 change: the iron hypothesis. Paleoceanography 5, 1–13.

Martin, J.H., Knauer, G.A., Karl, D.M., Broenkow, W.W., 1987. VERTEX: carbon cycling in the northeast Pacific. Deep-Sea Research 34 (2), 267–285.

McCarthy, J.J., Garside, C., Nevins, J.L., Barber, R.T., 1996. New production along 140°W in the equatorial Pacific during and following the 1992 El Niño event. Deep-Sea Research II 43 (4–6), 1065–1094.

Murray, J.W., Johnson, E., Garside, C., 1995. A U.S. JGOFS process study in the equatorial Pacific (EqPac): introduction. Deep-Sea Research II 42 (2–3), 275–293.

Murray, J.W., Young, J., Newton, J., Dunne, J., Chapin, T., Paul, B., McCarthy, J.J., 1996. Export flux of particulate organic carbon from the central equatorial Pacific determined using a combined drifting trap-^{234}Th approach. Deep-Sea Research II 43 (4–6), 1095–1132.

Nelson, D.M., Goering, J.J., 1977. Near-surface silica dissolution in the upwelling region off northwest Africa. Deep-Sea Research 24, 65–73.

Nelson, D.M., Goering, J.J., Boisseau, D.W., 1981. Consumption and regeneration of silicic acid in three coastal upwelling systems. In: Richards, F.A. (Ed.), Coastal Upwelling. American Geophysical Union, Washington, DC, pp. 242–256.

Nelson, D.M., Treguer, P., Brzezinski, M.A., Leynaert, A., Queguiner, B., 1995. Production and dissolution of biogenic silica in the ocean: revised global estimates, comparison with regional data and relationship to biogenic sedimentation. Global Biogeochemical Cycles 9 (3), 359–372.

Pacanowski, R.C., Dixon, K., Rosati, A., 1991. The GFDL modular ocean model user guide. The GFDL Ocean Group Technical Report No. 2, Geophysical Fluid Dynamics Laboratory, Princeton, USA.

Peña, M.A., Lewis, M.R., Harrison, W.G., 1990. Primary productivity and size structure of phytoplankton biomass on a transect of the equator at 135°W in the Pacific Ocean. Deep-Sea Research 37 (2), 295–315.

Philander, S.G., 1990. El Niño, La Niña, and the Southern Oscillation, Academic Press, Inc. 288pp.

Ragueneau, O., Treguer, P., Leynaert, A., Anderson, R.F., Brzezinski, M.A., Demaster, D.J., Dugdale, R.C., et al., 2000. A review of the Si cycle in the modern ocean: recent progress and missing gaps in the application of biogenic opal as a paleoproductivity proxy. Global and Planetary Change 26, 317–365.

Raimbault, P., Slawyk, G., Boudjellal, B., Coatanoan, C., Conan, P., Coste, B., Garcia, N., Moutin, T., Pujo-Pay, M., 1999. Carbon and nitrogen uptake and export in the equatorial Pacific at 150°W: evidence of an efficient regenerated production cycle. Journal of Geophysical Research 104 (C2), 3341–3356.

Sarmiento, J.L., Slater, R.D., Fasham, M.J.R., Ducklow, H.W., Toggweiler, J.R., Evans, G.T., 1993. A seasonal three-dimensional ecosystem model of nitrogen cycling in the North Atlantic euphotic zone. Global Biogeochemical Cycles 7, 417–450.

Strutton, P.G., Chavez, F.P., 2000. Primary productivity in the equatorial Pacific during the 1997–1998 El Niño. Journal of Geophysical Research 105 (C11), 26089–26102.

Takahashi, T., Sutherland, S.C., Sweeney, C., Poisson, A., Metzl, N., Tilbrook, B., Bates, N., Wanninkhof, R., Feely, R.A., Sabine, C., Olafsson, J., Nojiri, Y., 2002. Global sea–air CO_2 flux based on climatological surface ocean pCO_2 and seasonal biological and temperature effects. Deep-Sea Research II 49, 1601–1622.

Takeda, S., 1998. Influence of iron availability on nutrient consumption ratio of diatoms in oceanic water. Nature 393, 774–777.

Toggweiler, J.R., Carson, S., 1995. What are the upwelling systems contributing to the ocean's carbon and nutrient budgets. In: Summerhayes, C.P., et al. (Ed.), Upwelling in the Ocean: Modern Processes and Ancient Records. Wiley, New York, pp. 337–360.

Tréguer, P., Pondaven, P., 2000. Silica control of carbon dioxide. Nature 406, 358–359.

Tréguer, P., Nelson, D.M., Van Bennekom, A.J., DeMaster, D.J., Leynaert, A., Queguiner, B., 1998. The silica balance in the world ocean : a reestimate. Science 268, 1995.

Ward, B.B., 2000. Nitrification and the marine nitrogen cycle. In: Kirchman, D.L. (Ed.), Microbial Ecology of the Oceans. Wiley, New York, pp. 427–453.

Weisberg, R.H., Qiao, L., 2000. Equatorial upwelling in the central Pacific estimated from moored velocity profilers. Journal of Physical Oceanography 30, 105–124.

Wilkerson, F.P., Dugdale, R.C., 1992. Measurements of nitrogen productivity in the equatorial Pacific. Journal of Geophysical Research 97 (C1), 669–679.

Wyrtki, K., Kilonsky, B., 1984. Mean water and current structure during the Hawaii-Tahiti Shuttle Experiment. Journal of Physical Oceanography 14, 242–254.

Zhang, J., Quay, P.D., 1997. The total organic carbon export rate based on ^{13}C and ^{12}C of DIC budgets in the equatorial Pacific region. Deep-Sea Research II 44 (9–10), 2163–2190.